

Non-Equilibrium Quantum Spin Dynamics from Classical Stochastic Processes

S. De Nicola,¹ B. Doyon,² and M. J. Bhaseen³

¹*IST Austria, Am Campus 1, 3400 Klosterneuburg, Austria*

²*Department of Mathematics, King's College London, Strand, London WC2R 2LS, United Kingdom*

³*Department of Physics, King's College London, Strand, London WC2R 2LS, United Kingdom*

Following on from our recent work, we investigate a stochastic approach to non-equilibrium quantum spin systems. We show how the method can be applied to a variety of physical observables and for different initial conditions. We provide exact formulae of broad applicability for the time-dependence of expectation values and correlation functions following a quantum quench in terms of averages over classical stochastic processes. We further explore the behavior of the classical stochastic variables in the presence of dynamical quantum phase transitions, including results for their distributions and correlation functions. We provide details on the numerical solution of the associated stochastic differential equations, and examine the growth of fluctuations in the classical description. We discuss the strengths and limitations of the current implementation of the stochastic approach and the potential for further development.

I. INTRODUCTION

The experimental realization of isolated quantum many-body systems [1–6] has led to intense theoretical interest in their unitary time-evolution [7, 8]. The study of quantum quenches [9, 10] has provided fundamental insights into their non-equilibrium behavior, including the absence of thermalization in low-dimensional integrable systems [1, 11] and the role of the Generalized Gibbs Ensemble (GGE) [12–14]. This has stimulated the development of new theoretical tools and methodologies, ranging from the quench action approach [15, 16] to recent applications of hydrodynamics [17–21]. This has been complemented by significant advances in numerical simulation techniques [22–27]. The theoretical prediction of dynamical quantum phase transitions (DQPTs) [28, 29], which occur as a function of time, has been recently confirmed using trapped ions [30]. These experiments provide a new set of tools for exploring the time-resolved dynamics of quantum many-body systems using paradigmatic spin Hamiltonians.

Recently, a theoretical approach to quantum spin systems has emerged, based on a mapping to classical stochastic processes [31–34]. The procedure begins by decoupling the exchange interactions between spins using Hubbard–Stratonovich transformations. This yields an exact description in terms of independent quantum spins, where the effect of interactions is represented by Gaussian distributed stochastic fields. Quantum expectation values are then expressed as classical averages over these stochastic fields. In recent work [34], we showed that this approach could be used to calculate the expectation values of time-dependent quantum observables, including the experimentally measurable Loschmidt rate function and the magnetization. We also verified that this approach could handle both integrable and non-integrable models, including those in higher dimensions. Here, we extend our previous work in a number of directions, providing results for a broader range of observables under different initial conditions. We also present more in-

formation on the stochastic approach itself and its numerical implementation. We also present new results on the dynamics of the classical stochastic variables, including stochastic bounds on the Loschmidt rate function. For other recent work exploring the connections between quantum and classical dynamics see Refs [35–37].

The layout of this paper is as follows. In Section II we recall the principal steps involved in the stochastic approach to quantum spin systems, adopting the notations of Refs [33, 34]. In Section III we show how quantum observables can be computed in the stochastic formalism providing results of general applicability for spin-1/2 systems. In Section IV we illustrate the method by considering quenches in the quantum Ising model, in one and two spatial dimensions. In Section V we investigate the relationship between DQPTs and the classical stochastic variables. In Sections VI and VII we discuss the strengths and limitations of the stochastic approach, exploring the growth of fluctuations in the classical variables and the computational cost of numerical simulations. We conclude in Section VIII, summarizing our findings and indicating directions for future research. We also provide appendices on the technical details of the stochastic approach and its numerical implementation.

II. STOCHASTIC FORMALISM

In this section we recall the principal steps involved in the stochastic approach to quantum spin systems [31–34]. Following Refs [33, 34], we begin our discussion with a generic Heisenberg Hamiltonian

$$\hat{H} = - \sum_{ijab} \mathcal{J}_{ij}^{ab} \hat{S}_i^a \hat{S}_j^b - \sum_{ja} h_j^a \hat{S}_j^a, \quad (1)$$

where i, j indicate lattice sites and a, b label the spin components. The spin operators satisfy the $su(2)$ commutation relations $[\hat{S}_j^a, \hat{S}_k^b] = i\epsilon^{abc}\delta_{jk}\hat{S}_k^c$, where $a, b, c \in \{x, y, z\}$, ϵ^{abc} is the antisymmetric symbol and we set $\hbar = 1$. The exchange interactions \mathcal{J}_{ij}^{ab} and the fields

h_j^a can, in general, be time-dependent. Away from equilibrium, unitary dynamics under \hat{H} is governed by the time-evolution operator

$$\hat{U}(t_f, t_i) = \mathbb{T} \exp \left(-i \int_{t_i}^{t_f} dt \hat{H}(t) \right), \quad (2)$$

where t_i and t_f denote the initial and final times, and \mathbb{T} denotes time-ordering. In general, the time-evolution operator $\hat{U}(t_f, t_i)$ is non-trivial, due to the quadratic spin interactions in \hat{H} , the non-commutativity of the spin operators, and the time-ordering. However, some of these difficulties can be circumvented in a two-step process. First, the quadratic spin interactions in \hat{H} can be decoupled exactly using Hubbard–Stratonovich (HS) transformations. This leads to a physically appealing description in terms of independent quantum spins which are coupled via Gaussian distributed stochastic “magnetic” fields [31, 33]. Second, the time-ordered exponential in Eq. (2) can be recast as an ordinary exponential; the HS decoupling renders the exponent linear in the $su(2)$ generators, allowing a simpler parameterization via group theory [32, 33]. This so-called *disentanglement transformation* [33, 34] can be regarded as a judicious parameterization of the time-evolution operator which takes advantage of the Lie algebraic structure of the spin operators. In Sections II A and II B we recall these two steps in turn, before summarizing the resulting stochastic differential equations (SDEs) [33, 34]. In Section II C we discuss the Ito form of these SDEs, which is useful for numerical simulations.

A. Hubbard–Stratonovich Transformation

As in Refs [31–34], the quadratic spin interactions can be decoupled via a HS transformation [38, 39] over auxiliary variables φ_j^a . Trotter slicing [40] the exponential in Eq. (2) and applying the HS transformation at each time slice (Appendix A) one obtains

$$\hat{U}(t_f, t_i) = \mathbb{T} \int \mathcal{D}\varphi e^{-S[\varphi] + i \int_{t_i}^{t_f} \sum_{ja} \Phi_j^a(t') \hat{S}_j^a dt'}, \quad (3)$$

where we refer to

$$S[\varphi] = \sum_{ijab} \int_{t_i}^{t_f} \frac{1}{4} (\mathcal{J}^{-1})_{ij}^{ab} \varphi_i^a(t') \varphi_j^b(t') dt', \quad (4)$$

as the *noise action*. Here, we define $\Phi_j^a \equiv h_j^a + \varphi_j^a/\sqrt{i}$ and further denote

$$\mathcal{D}\varphi \equiv \prod_j \mathcal{D}\varphi_j^a, \quad (5)$$

where $\mathcal{D}\varphi_j^a$ is the appropriately normalized integration measure for each HS variable φ_j^a . Introducing the change of variables $\varphi_i^a = \sum_{jb} O_{ij}^{ab} \phi_j^b$, where $O^T \mathcal{J}^{-1} O/2 = \mathbb{1}$ and

$\mathbb{1}$ is the identity matrix, the noise action in Eq. (4) can be recast in the diagonal form

$$S[\phi] = \sum_{ia} \int_{t_i}^{t_f} \frac{1}{2} \phi_i^a(t') \phi_i^a(t') dt', \quad (6)$$

where ϕ_i^a are real-valued Gaussian white noise variables satisfying $\langle \phi_i^a(t) \rangle = 0$, $\langle \phi_i^a(t) \phi_j^b(t') \rangle = \delta(t-t') \delta_{ij} \delta_{ab}$; see Appendix B. This yields a probabilistic interpretation of Eq. (3) as an integral over Gaussian weighted stochastic paths $\phi_i^a(t)$ [31, 33]. The time-evolution operator can thus be written in the form

$$\hat{U}(t_f, t_i) = \langle \mathbb{T} e^{i \int_{t_i}^{t_f} \sum_{ja} \Phi_j^a(t') \hat{S}_j^a dt'} \rangle_\phi, \quad (7)$$

where $\Phi_j^a = h_j^a + \sum_{kb} O_{jk}^{ab} \phi_k^b/\sqrt{i}$ and $\langle \dots \rangle_\phi$ denotes averaging with respect to the Gaussian weight given by Eq. (6). Equivalently, Eq. (7) describes the time-evolution of individual decoupled spins moving under the action of applied and stochastic “magnetic” fields, $h_j^a(t)$ and $\check{h}_j^a(t) \equiv \varphi_j^a/\sqrt{i} = \sum_{kb} O_{jk}^{ab} \phi_k^b(t)/\sqrt{i}$, respectively. Although the spins appear to be fully decoupled in the representation (7), the effect of the interactions is encoded in the fields $\check{h}_j^a(t)$ via the matrix O_{jk}^{ab} . Each spin is governed by an effective stochastic Hamiltonian

$$\hat{H}_j^s(t) = - \sum_a (h_j^a(t) + \check{h}_j^a(t)) \hat{S}_j^a. \quad (8)$$

In general, this is non-Hermitian, as the stochastic fields \check{h}_j^a may be complex valued. Without loss of generality, in the remainder of this work we consider time-evolution over the interval $[0, t]$ and set $\hat{U}(t) \equiv \hat{U}(t, 0)$.

B. Disentanglement Transformation

The time-evolution operator defined by Eq. (7) is still non-trivial due to the time-ordering operation. However the decoupled exponential is now linear in the spin operators, and can therefore be simplified using group theory [31–33]. Specifically, one may rewrite the time-evolution operator acting at a given site j as

$$\mathbb{T} e^{i \sum_a \int_0^t \Phi_j^a(t') \hat{S}_j^a dt'} \equiv e^{\xi_j^+(t) \hat{S}_j^+} e^{\xi_j^z(t) \hat{S}_j^z} e^{\xi_j^-(t) \hat{S}_j^-}, \quad (9)$$

where the parameters $\xi_j^a(t)$ are referred to as *disentangling variables* [33]. This is also known as the Wei–Norman–Kolokolov transformation [41, 42]. The relationship between the disentangling variables $\xi_j^a(t)$ and the variables $\Phi_j^a(t)$ can be made more explicit by differentiating Eq. (9) with respect to time. This yields [33]

$$i\dot{\xi}_j^+ = \Phi_j^+ + \Phi_j^z \xi_j^+ - \Phi_j^- \xi_j^{+2}, \quad (10a)$$

$$i\dot{\xi}_j^z = \Phi_j^z - 2\Phi_j^- \xi_j^+, \quad (10b)$$

$$i\dot{\xi}_j^- = \Phi_j^- \exp \xi_j^z, \quad (10c)$$

where the identity $\hat{U}(0) = 1$ implies the initial conditions $\xi_j^a(0) = 0$ for all j, a . For completeness, we provide a detailed derivation of these equations in Appendix C. Alternative disentanglement transformations, based on different group parameterizations, have also been considered in the literature [31, 33].

Equations (10) may be regarded as stochastic differential equations (SDEs) for the variables ξ_j^a , due to the presence of the (additive and multiplicative) Gaussian noise entering via Φ_j^a [33]. Applying the disentanglement transformation (10) to the time-evolution operator (7) one obtains [33, 34]

$$\hat{U}(t) = \langle \otimes_j \hat{U}_j^s(t) \rangle_\phi, \quad (11)$$

where we have defined on-site stochastic operators

$$\hat{U}_j^s(t) \equiv e^{\xi_j^+(t)\hat{S}_j^+} e^{\xi_j^z(t)\hat{S}_j^z} e^{\xi_j^-(t)\hat{S}_j^-}. \quad (12)$$

In general, this is a non-unitary operator, since the time-evolution of each spin is governed by the non-Hermitian Hamiltonian (8). Given a specific spin representation, $\hat{U}_j^s(t)$ can be written in matrix form. For example, for spin- $\frac{1}{2}$, we may write $\hat{S}^a = \hat{\sigma}^a/2$ in terms of the Pauli matrices $\hat{\sigma}^a$, where $a \in \{x, y, z\}$. This yields

$$\hat{U}_j^s(t) = \begin{pmatrix} e^{\xi_j^z/2} + e^{-\xi_j^z/2} \xi_j^+ \xi_j^- & e^{-\xi_j^z/2} \xi_j^+ \\ e^{-\xi_j^z/2} \xi_j^- & e^{-\xi_j^z/2} \end{pmatrix}. \quad (13)$$

The product form of the evolution operator (11) makes it convenient for acting on spin states of interest; using this, the quantum matrix elements of an operator $\hat{O}(t) \equiv \hat{U}^\dagger(t)\hat{O}\hat{U}(t)$ can be expressed as the classical average of a function $f(\xi)$, over realizations of the stochastic process:

$$\langle \psi_F | \hat{O}(t) | \psi_I \rangle = \langle f(\xi(t)) \rangle_\phi. \quad (14)$$

Here, the function $f(\xi)$ depends on the disentangling variables $\xi \equiv \{\xi_j^a\}$, and is determined by the observable \hat{O} , and the chosen initial and final states, $|\psi_I\rangle$ and $|\psi_F\rangle$. In writing (14), we consider operators \hat{O} without explicit time-dependence: in the Heisenberg picture their time-evolution is determined solely by $\hat{U}(t)$. In the Schrödinger picture, the matrix elements can be recast as $\langle \psi_F(t) | \hat{O} | \psi_I(t) \rangle$, where $|\psi(t)\rangle \equiv \hat{U}(t)|\psi(0)\rangle$. In Section III we will provide some explicit examples of the quantum-classical correspondence (14), for different observables and for different initial and final states.

C. Ito Equations of Motion

SDEs are defined by specifying a discretization scheme [43], with the most common choices being the Ito and Stratonovich conventions. The SDEs (10) are initially in the Stratonovich form. However, for numerical simulations, it is often convenient to work with the Ito form of

the SDEs, which are naturally suited for discrete time-evolution. The Ito SDEs can be obtained by including an extra drift term. However, in the case of an interaction matrix \mathcal{J}_{ij}^{ab} with vanishing diagonal elements, the additional Ito drift term vanishes identically and the Ito and Stratonovich SDEs coincide; see Appendix D. The time-dependence of a function $f(\xi)$ corresponding to a physical observable $\hat{O}(t)$ can be found via Ito calculus. For a generic Ito SDE written in the canonical form,

$$\frac{d\xi_i^a}{dt} = A_i^a(\xi) + \sum_{jb} B_{ij}^{ab}(\xi)\phi_j^b, \quad (15)$$

one obtains

$$\dot{f} = \sum_{ia} \frac{\partial f}{\partial \xi_i^a} (A_i^a + \sum_{jb} B_{ij}^{ab} \phi_j^b) + \frac{1}{2} \sum_{ijab} \frac{\partial^2 f}{\partial \xi_i^a \partial \xi_j^b} \sum_{ck} B_{ik}^{ac} B_{jk}^{bc}, \quad (16)$$

as follows from Ito's lemma [43]. In principle, it is possible to analytically average these SDEs with respect to the HS fields; in this approach, one obtains a system of ordinary differential equations (ODEs) [33]. However, as we discuss in Appendix E, this is formally equivalent to diagonalizing the Hamiltonian, whose matrix dimension scales as $\mathcal{O}(2^N \times 2^N)$, where N is the total number of spins. Instead, it is more convenient to numerically perform the average in (14) over independent realizations of the stochastic process. In this approach, the number of stochastic variables ξ_j^a that one needs to simulate scales linearly with N . Moreover, the independent runs can be readily parallelized. In Section III, we will provide exact stochastic formulae for a variety of quantum observables that can be described in this way. We will return to a more detailed discussion of the numerical aspects in Sections VI and VII.

III. QUANTUM OBSERVABLES

In order to illustrate the stochastic approach to non-equilibrium quantum spin systems, we obtain below the classical formulae for a range of quantum observables.

A. Loschmidt Amplitude

One of the simplest quantities to investigate in the stochastic formalism is the Loschmidt amplitude $A(t)$. This is defined as the amplitude for an initial state $|\psi(0)\rangle$ to return to itself after unitary evolution [28]:

$$A(t) = \langle \psi(0) | \hat{U}(t) | \psi(0) \rangle. \quad (17)$$

In general, $A(t)$ is expected to decay exponentially with the system size N . It is therefore convenient to define the Loschmidt rate function

$$\lambda(t) \equiv -\frac{1}{N} \log |A(t)|^2. \quad (18)$$

This plays the role of a dynamical free energy density, since $A(t)$ is analogous to a boundary partition function [44] that is Wick-rotated to real time. This connection led to the insightful prediction of dynamical quantum phase transitions (DQPTs) occurring in $\lambda(t)$ as a function of time [28]. In the thermodynamic limit $N \rightarrow \infty$, these transitions correspond to non-analyticities in $\lambda(t)$, and often occur on quenching across a quantum critical point [28, 29]. The existence of DQPTs has been recently confirmed in experiment using trapped ions [30]. This experiment provides a realization of the quantum Ising model with 6 to 10 spins, interacting via tunable dipolar interactions. This allows access to the time-resolved dynamics of an isolated quantum spin system.

Here, we consider $A(t)$ for the generic Hamiltonian (1). In principle, this may contain long range interactions as in the experiment [30], but this is not the primary thrust of our investigation. For simplicity, we focus on initial states of product form, $|\psi(0)\rangle = \otimes_i |\psi(0)\rangle_i$. Parameterizing a generic superposition as $|\psi(0)\rangle_i = a_i |\uparrow\rangle_i + b_i |\downarrow\rangle_i$, where $|\uparrow\rangle$ and $|\downarrow\rangle$ refer to spin-up and spin-down in the \hat{S}_i^z basis, with $|a_i|^2 + |b_i|^2 = 1$, one obtains

$$A(t) = \left\langle \prod_i e^{-\frac{\xi_i^z}{2}} \left(|a_i|^2 e^{\xi_i^z} + (a_i \xi_i^- + b_i)(a_i^* \xi_i^+ + b_i^*) \right) \right\rangle_{\phi} \quad (19)$$

In the special case of a fully-polarized initial state $|\Downarrow\rangle$ with all spins down, corresponding to $a_i = 0$ and $b_i = 1$, one obtains the result given in our previous work [34]. The result (19) is more general and allows consideration of spatially inhomogeneous initial states. In Section IV we will discuss the numerical evaluation of (19) in the context of the quantum Ising model, including domain wall initial conditions. For now, we gather the stochastic formulae describing local observables.

B. One-Point Functions

The dynamics of a local observable \hat{O} is encoded in the time-dependent expectation value

$$\langle \hat{O}(t) \rangle = \langle \psi(0) | \hat{U}^\dagger(t) \hat{O} \hat{U}(t) | \psi(0) \rangle. \quad (20)$$

for quenches starting in $|\Downarrow\rangle$. The structure of (22) mirrors that of (21), where now there are two polynomial factors with minus signs, for the chosen sites i and j . This result is readily generalized to arbitrary multi-point functions of the local magnetization, starting in the state $|\Downarrow\rangle$; the

In contrast to the Loschmidt amplitude (17), this involves two time-evolution operators. This can be addressed by two independent HS transformations over variables $\phi \equiv \{\phi_i^a\}$ and $\tilde{\phi} \equiv \{\tilde{\phi}_i^a\}$, with associated disentanglement variables $\xi \equiv \{\xi_i^a[\phi]\}$ and $\tilde{\xi} \equiv \{\tilde{\xi}_i^a[\tilde{\phi}]\}$. For simplicity, we illustrate this in the case where the observable \hat{O} of interest is a product of \hat{S}_i^z operators at different sites. This class of operators includes the longitudinal magnetization as well as correlation functions. For product initial states, the argument of the classical average is factorized over the sites i . A given observable \hat{O} can then be expressed in the stochastic language by multiplying a set of on-site “building blocks”, given in Appendix F. In this framework, local expectation values are expressed as averages of functions of ξ and $\tilde{\xi}$, describing the forwards and backwards evolutions respectively. For example, the dynamics of the local magnetization for a system initialized in the state $|\psi(0)\rangle = |\Downarrow\rangle$ is given by [34]

$$\langle \hat{S}_i^z(t) \rangle = -\frac{1}{2} \left\langle e^{-\sum_j \left(\frac{\xi_j^z + \tilde{\xi}_j^{z*}}{2} \right)} (1 - \xi_i^+ \tilde{\xi}_i^{+*}) \prod_{j \neq i} (1 + \xi_j^+ \tilde{\xi}_j^{+*}) \right\rangle_{\phi, \tilde{\phi}}. \quad (21)$$

The structure of (21) is relatively straightforward. It consists of an exponential factor like that in (19), together with polynomial factors $(1 \pm \xi_j^+ \tilde{\xi}_j^{+*})$ for each site, where the minus sign is used for the chosen site i . As discussed in Section III C, a similar structure also emerges in the evaluation of correlation functions. Analogous results for $\langle S_i^\alpha(t) \rangle$ with $\alpha = x, y$ are given in Appendix F.

C. Equal-Time Correlation Functions

Correlation functions of local operators can be computed in a similar manner to that described above. For example, the two-point function of the local magnetization $C_{ij}(t) \equiv \langle \hat{S}_i^z(t) \hat{S}_j^z(t) \rangle$ is given by

$$C_{ij}(t) = \frac{1}{4} \left\langle e^{-\sum_k \left(\frac{\xi_k^z + \tilde{\xi}_k^{z*}}{2} \right)} (1 - \xi_i^+ \tilde{\xi}_i^{+*}) (1 - \xi_j^+ \tilde{\xi}_j^{+*}) \prod_{k \neq i, j} (1 + \xi_k^+ \tilde{\xi}_k^{+*}) \right\rangle_{\phi, \tilde{\phi}}, \quad (22)$$

sign of the polynomial is negative for each factor of \hat{S}_i^z in the correlation function. More generally, the expectation value of a product of local operators starting from a product state can be decomposed into averages of products of the elementary “building blocks” referred to above; see

Appendix F. In the case of an initial state $|\Downarrow\rangle$, equations (21) and (22) can be equivalently decomposed into a “background” factor $\prod_j e^{-\sum_j(\xi_j^z + \tilde{\xi}_j^{z*})/2}(1 + \xi_j^+ \tilde{\xi}_j^{+*})$, for all the sites that are not involved in the observable, together with a multiplicative factor for each inserted local operator. This structure is reminiscent of the form of correlation functions obtained from the algebraic Bethe ansatz, see e.g. Ref. [45], although the present results apply to both integrable and non-integrable problems.

D. Dynamical Correlation Functions

Dynamical correlation functions involving operators at different times can also be expressed in the stochastic

formalism, by decoupling each of the time-evolution operators. For example, the two-time correlation function $C_{ij}(t, t') \equiv \langle \hat{S}_i^z(t) \hat{S}_j^z(t') \rangle$ can be written as

$$C_{ij}(t, t') = \langle \psi(0) | \hat{U}^\dagger(t) \hat{S}_i^z \hat{U}(t) \hat{U}^\dagger(t') \hat{S}_j^z \hat{U}(t') | \psi(0) \rangle. \quad (23)$$

Starting in the initial state $|\psi(0)\rangle = |\Downarrow\rangle$ and using $\hat{U}(t) \hat{U}^\dagger(t') = \hat{U}(t - t')$, one obtains

$$C_{ij}(t, t') = \frac{1}{4} \left\langle e^{-\frac{1}{2} \sum_i (\xi_{1,i}^-(t)^* + \xi_{2,i}^z(t-t') + \xi_{3,i}^z(t'))} \left[(\xi_{2,i}^-(t-t') \xi_{3,i}^+(t') + 1) \left(\xi_{2,i}^+(t-t') \xi_{1,i}^+(t)^* - 1 \right) + \xi_{3,i}^+(t') e^{\xi_{2,i}^z(t-t')} \xi_{1,i}^+(t)^* \right] \right. \\ \left. \left[(\xi_{2,j}^-(t-t') \xi_{3,j}^+(t') - 1) \left(\xi_{2,j}^+(t-t') \xi_{1,j}^+(t)^* + 1 \right) + \xi_{3,j}^+(t') e^{\xi_{2,j}^z(t-t')} \xi_{1,j}^+(t)^* \right] \times \right. \\ \left. \prod_{k \neq i,j} \left(\xi_{1,k}^+(t)^* \left(\xi_{2,k}^-(t-t') \xi_{2,k}^+(t-t') \xi_{3,k}^+(t') + \xi_{2,k}^+(t-t') + \xi_{3,k}^+(t') e^{\xi_{2,k}^z(t-t')} \right) + \xi_{2,k}^-(t-t') \xi_{3,k}^+(t') + 1 \right) \right\rangle_{\phi_1, \phi_2, \phi_3}. \quad (24)$$

Here we have introduced three sets of disentangling variables $\xi_{1,2,3}$ which are functionals of three independent Gaussian white noise fields $\phi_{1,2,3}$. Although the expression (24) is rather non-trivial, it is general to dynamical correlations of arbitrary spin-1/2 Heisenberg models (1), without reference to integrability or dimensionality.

E. Higher Dimensions

A notable feature of the stochastic approach is that it applies to systems in arbitrary dimensions. Due to the on-site character of the stochastic time-evolution operators $\hat{U}_j^s(t)$, all of the formulae obtained above readily generalize to arbitrary dimensions: the products simply extend over all the lattice sites. In Section IV we will provide an example of this in the context of the two-dimensional quantum Ising model.

IV. QUANTUM ISING MODEL

In order to illustrate how the stochastic method can be applied in practice, we consider quantum quenches in the one-dimensional (1D) quantum Ising model [34]. The Hamiltonian is given by

$$\hat{H}_I = -J \sum_{j=1}^N \hat{S}_j^z \hat{S}_{j+1}^z - \Gamma \sum_{j=1}^N \hat{S}_j^x, \quad (25)$$

where $J > 0$ is the ferromagnetic nearest neighbor exchange interaction and Γ is the transverse field. For simplicity, we consider periodic boundary conditions with $\hat{S}_{N+1}^a = \hat{S}_1^a$. In equilibrium, the model (25) exhibits a quantum phase transition at $\Gamma = \Gamma_c \equiv J/2$ between a ferromagnetic (FM) phase for $\Gamma < \Gamma_c$ and a paramagnetic (PM) phase for $\Gamma > \Gamma_c$. Out of equilibrium, the dynamics of the Hamiltonian (25) is encoded in the Ito SDEs

$$-i\dot{\xi}_j^+ = \frac{\Gamma}{2}(1 - \xi_j^{+2}) + \xi_j^+ \sum_k O_{jk} \phi_k / \sqrt{i}, \quad (26a)$$

$$-i\dot{\xi}_j^z = -\Gamma \xi_j^+ + \sum_k O_{jk} \phi_k / \sqrt{i}, \quad (26b)$$

$$-i\dot{\xi}_j^- = \frac{\Gamma}{2} \exp \xi_j^z, \quad (26c)$$

where O_{jk} is defined by $\sum_{kl} O_{ki} \mathcal{J}_{kl}^{-1} O_{lj} = 2\delta_{ij}$, and we take a symmetrized interaction matrix $\mathcal{J}_{ij} = \frac{J}{2}(\delta_{ij+1} + \delta_{ij-1})$ [46]. Before embarking on a detailed examination of (26), it is instructive to consider some limiting cases. In the non-interacting limit $J = 0$, one has $O_{jk} = 0$, and (26) reduces to a set of deterministic equations which can be solved exactly. As expected, these describe a set of decoupled spins precessing in an external magnetic field Γ ; see Appendix G. In the limit $\Gamma = 0$, the model (25) is purely classical. In this case $\xi_j^\pm(t) = 0$ for all t , while $\xi_j^z(t)$ undergoes exactly solvable Brownian motion; see Appendix G. For generic values of Γ and J , the

SDEs (26) can be solved numerically, as we highlighted in our previous work [34].

Throughout this manuscript, we solve the SDEs using the Euler scheme [43]. We also set $J = 1$ and use a discrete time-step $\Delta t = 10^{-5}$ in all of the figures. For any non-zero Δt , numerical solution algorithms for non-linear SDEs can give rise to diverging trajectories where the stochastic variables grow without bound [43, 47]; for the Ising SDEs, this effect is most pronounced for large transverse fields Γ . Empirically, trajectories are found to monotonically grow to numerical infinity when

$$|\dot{\xi}_i^+(t)|\Delta t \geq |\xi_i^+(t)|, \quad (27)$$

i.e. when the increment in $|\xi_i^+(t)|$ in a given time-step exceeds the value of $|\xi_i^+(t)|$. In the case of the Ising model, the increment is given by Eq. (26a). Since the fields ϕ_i are of order one and $\Gamma\Delta t$ is typically small, Eq. (27) can only be satisfied for large $|\xi_i^+|$. The increment is then dominated by the term proportional to $|\xi_i^{+2}|$, and the requirement (27) translates into a divergence condition $|\dot{\xi}_i^+(t)| > \xi_c^+$, where $\xi_c^+ \equiv 2/\Gamma\Delta t$. Diverging trajectories can therefore be identified by comparing $\xi_i^+(t)$ to ξ_c^+ at each time t . With our choice of Δt , we retain between 99% and 100% of the total number of trajectories, depending on the chosen parameters. The stochastic averages are performed by retaining only the non-diverging trajectories at a given time t . Whenever trajectories are excluded, we report their relative fraction in the associated figure caption. We estimate the magnitude of the fluctuations on our results via the standard error $s_e = \sigma/\sqrt{n_B}$, where σ is the standard deviation obtained by splitting the data into $n_B = 5$ batches of trajectories; we omit the bars when they are comparable to, or smaller than, the plot points. In order to illustrate the general approach, we focus on relatively small system sizes with $N \leq 10$ spins. This aids comparison with Exact Diagonalization (ED) using the QuSpin package [48] and reduces the computational cost, whilst exposing the main features. We also confine ourselves to times $t \lesssim 1/J$, before stochastic fluctuations become important. In Sections VI and VII we will examine the scaling of the method with increasing N and discuss the eventual breakdown with increasing t .

A. Loschmidt Amplitude

In order to illustrate the general approach, we begin by considering the Loschmidt amplitude for different quantum quenches. For systems initialized in the fully-polarized state $|\Downarrow\rangle \equiv \otimes_i |\downarrow\rangle_i$, corresponding to a FM ground state of the Hamiltonian (25) when $\Gamma = 0$, the general formula (19) reduces to

$$A(t) = \left\langle \prod_i \exp\left(-\frac{\xi_i^z(t)}{2}\right) \right\rangle_\phi, \quad (28)$$

as reported in our previous work [34]. In Fig. 1 we show the time-evolution of $\lambda(t)$ following a quench from $\Gamma = 0$

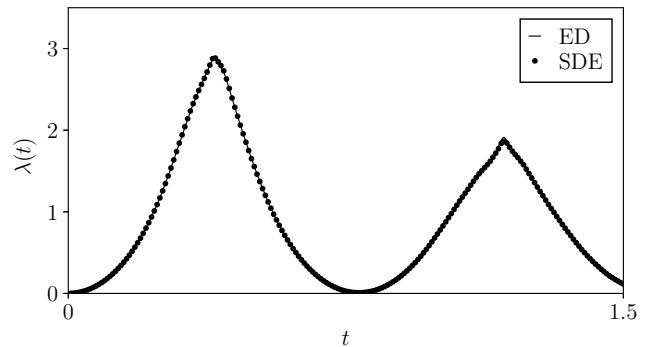


FIG. 1. Loschmidt rate function $\lambda(t)$ for the 1D quantum Ising model following a quantum quench from the fully-polarized initial state $|\Downarrow\rangle$ to the PM phase with $\Gamma = 16\Gamma_c$. The results obtained from the SDEs (filled circles) are in good agreement with ED (solid line) for $N = 9$ spins. The SDE results were obtained by averaging over 10^5 realizations of the stochastic process. The fraction of diverging trajectories at the stopping time is of order 1%.

to $\Gamma = 16\Gamma_c$, across the quantum phase transition at Γ_c . The results obtained from the numerical solution of the SDEs in (26) are in good agreement with ED. They also correctly reproduce the sharp peak in $\lambda(t)$ corresponding to a DQPT in the thermodynamic limit [28]. Going beyond our previous work [34], it is also possible to consider quenches from the PM phase to the FM phase. For example, for quenches starting in the PM ground state $|\rightarrow\rangle \equiv \otimes_i |\rightarrow\rangle_i$ for $\Gamma = \infty$, where $\hat{S}_i^x |\rightarrow\rangle_i = 1/2 |\rightarrow\rangle_i$, the general formula (19) reduces to

$$A(t) = \left\langle \prod_i \frac{1}{2} e^{-\frac{\xi_i^z}{2}} \left(\xi_i^- \xi_i^+ + \xi_i^- + \xi_i^+ + e^{\xi_i^z} + 1 \right) \right\rangle_\phi. \quad (29)$$

In Fig. 2 we show the time-evolution of $\lambda(t)$ following a quench from $\Gamma = \infty$ (PM) to $\Gamma = \Gamma_c/4$ (FM), computed from Eq. (29). Again, we find very good agreement with ED. It is worth noting that, in contrast to the simple result (28), the expression (29) features a sum of terms inside the average. However, from a computational standpoint, this only involves a linear increase in the number of operations required. Furthermore, the averaging need not be performed at each time-step: while for numerical accuracy the SDEs are solved with a small time-step (e.g. $\Delta t \approx 10^{-5}$), observables may be computed on a coarser time interval (e.g. $\Delta t \approx 10^{-3}$). The main computational cost of the method is associated with solving the SDEs, rather than performing the averages. Therefore, the presence of the additional terms in Eq. (29) does not significantly affect the computational cost: this applies to all the other examples considered in this Section. Finally, we note that Eq. (29) can be evaluated from the same set of trajectories as used in Eq. (28). Thus, in contrast with other numerical techniques such as time-dependent Density Matrix Renormalization Group (tDMRG) approaches or ED, the same data can be used

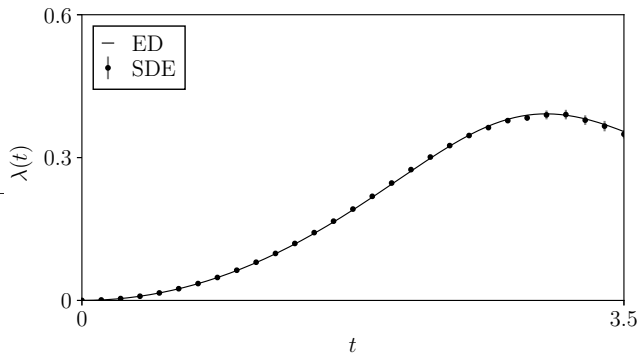


FIG. 2. Loschmidt rate function $\lambda(t)$ for the 1D quantum Ising model following a quantum quench from the initial state $|\Rightarrow\rangle$, corresponding to the paramagnetic ground state when $\Gamma = \infty$, to the FM phase with $\Gamma = \Gamma_c/4$. The results obtained from the SDEs (filled circles) are in good agreement with ED (solid line) for $N = 5$ spins. The SDE results were obtained by averaging over 10^5 realizations of the stochastic process.

to compute the time-evolution of different initial states.

As discussed in Section III A, the stochastic approach can also handle spatially inhomogeneous initial states. For example, we may consider domain wall initial condi-

tions:

$$|\psi(0)\rangle = |\uparrow\rangle_1 \otimes \dots \otimes |\uparrow\rangle_M \otimes |\downarrow\rangle_{M+1} \dots \otimes |\downarrow\rangle_N, \quad (30)$$

where $1 \leq M < N$. In this case

$$A(t) = \left\langle \prod_{j=1}^M \left(e^{\xi_j^z} + \xi_j^- \xi_j^+ \right) \prod_{i=1}^N e^{-\frac{\xi_i^z(t)}{2}} \right\rangle_{\phi}. \quad (31)$$

In Figs 3 and 4 we show the results for $\lambda(t)$ for different values of M , corresponding to a single spin flip and an extended domain of inverted spins respectively. Once again, the results are in good agreement with ED.

B. Magnetization Dynamics

A key observable for non-equilibrium quantum spin systems is the time-dependent magnetization $\mathcal{M}(t) = \sum_i^N \mathcal{M}_i(t)/N$ where $\mathcal{M}_i(t) = \langle \hat{S}_i^z(t) \rangle$. Here we consider quantum quenches from the initial state $|\Downarrow\rangle$ to different final values of Γ in the PM phase. As can be seen in Fig. 5, the results obtained by performing the stochastic average in (21) are in very good agreement with ED; here we focus on small system sizes with $N = 3$ spins as we need to average over two sets of disentangling variables, ξ_i and $\tilde{\xi}_i$. Again, we may consider different initial conditions, such as the inhomogeneous state (30). For example, for an initial state where the spin at site i is pointing up and every other spin is pointing down, the time-dependent magnetization at site i is given by

$$\mathcal{M}_i(t) = \langle \hat{S}_i^z(t) \rangle = -\frac{1}{2} \left\langle e^{-\sum_j \left(\frac{\xi_j^z + \tilde{\xi}_j^{z*}}{2} \right)} \left[(e^{\xi_i^z} + \xi_i^- \xi_i^+) (e^{\tilde{\xi}_i^z} + \tilde{\xi}_i^- \tilde{\xi}_i^{+*}) - \xi_i^- \tilde{\xi}_i^{-*} \right] \prod_{j \neq i} (1 + \xi_j^+ \tilde{\xi}_j^{+*}) \right\rangle_{\phi, \tilde{\phi}}, \quad (32)$$

where the disentangling variables ξ satisfy the Ising SDEs (26). This result can be obtained using the building blocks given in (F1) and (F2) of Appendix F.

A significant feature of the stochastic approach to non-equilibrium quantum spin systems is that it is not restricted to integrable models. A simple way to break the integrability of the quantum Ising model (25) is through the addition of a longitudinal magnetic field h , so that the Hamiltonian is given by $\hat{H} = \hat{H}_I + h \sum_j \hat{S}_j^z$. In the stochastic formalism the dynamics of this non-integrable model is described by the Ito SDEs

$$-i\dot{\xi}_j^+ = \frac{\Gamma}{2}(1 - \xi_j^{+2}) - h\xi_j^+ + \xi_j^+ \sum_k O_{jk} \phi_k / \sqrt{i}, \quad (33a)$$

$$-i\dot{\xi}_j^z = -h - \Gamma\xi_j^+ + \sum_k O_{jk} \phi_k / \sqrt{i}, \quad (33b)$$

$$-i\dot{\xi}_j^- = \frac{\Gamma}{2} \exp \xi_j^z, \quad (33c)$$

where O is the same as for the purely transverse field Ising model, as given in Section IV. In Fig. 6, we show results for $\mathcal{M}(t)$ corresponding to quenches from the fully-polarized initial state $|\Downarrow\rangle$ to different values of Γ , with h held fixed. Once again, we find very good agreement with ED. It is interesting to note that the same formula (21) governs the dynamics in both the integrable and non-integrable cases; the Hamiltonian enters only via the time-evolution of the disentangling variables ξ_i^a , not the function being averaged.

As discussed in our previous work [34], the stochastic approach can also be used in higher dimensions. For simplicity, we focus on the two-dimensional (2D) quantum Ising model with the Hamiltonian

$$\hat{H}_I^{2D} = -J \sum_{\langle ij \rangle} \hat{S}_i^z \hat{S}_j^z - \Gamma \sum_{\mathbf{i}} \hat{S}_{\mathbf{i}}^x, \quad (34)$$

where \mathbf{i} and \mathbf{j} indicate sites on a square lattice. In equi-

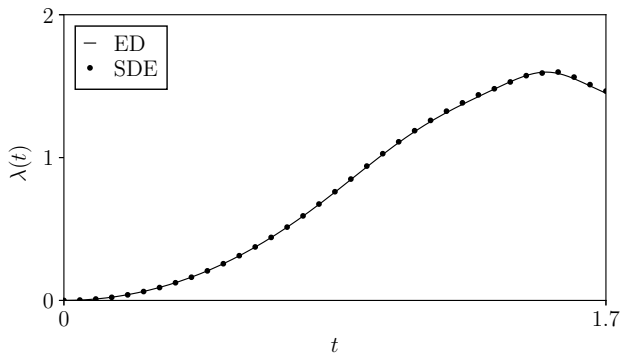


FIG. 3. Loschmidt rate function $\lambda(t)$ for the 1D quantum Ising model following a quantum quench from the spatially inhomogeneous initial state $|\uparrow\downarrow\downarrow\downarrow\rangle$ to the PM phase with $\Gamma = 4\Gamma_c$. The results obtained from the SDEs (filled circles) are in good agreement with ED (solid line) for $N = 5$ spins. The SDE results were obtained by averaging over 10^5 realizations of the stochastic process. Less than 0.1% of the trajectories were found to be divergent at the stopping time.

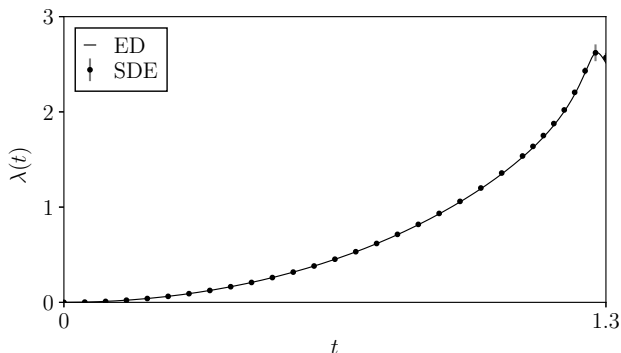


FIG. 4. Loschmidt rate function $\lambda(t)$ for the 1D quantum Ising model following a quantum quench from the spatially inhomogeneous initial state $|\uparrow\uparrow\downarrow\downarrow\rangle$ to the PM phase with $\Gamma = 4\Gamma_c$. The results obtained from the SDEs (filled circles) are in good agreement with ED (solid line) for $N = 5$ spins. The SDE results were obtained by averaging over 10^5 realizations of the stochastic process. Less than 0.1% of the trajectories were found to be divergent at the stopping time. Larger error bars are visible in the vicinity of the peak, due to the presence of enhanced stochastic fluctuations.

librium, this model exhibits a quantum phase transition when $\Gamma = \Gamma_c^{2D} \approx 1.523J$ [49, 50]. In Fig. 7 we show results for the magnetization dynamics $\mathcal{M}(t)$ following a quantum quench from the fully-polarized initial state $|\downarrow\rangle$ to $\Gamma \approx 5.3\Gamma_c^{2D}$. Again, the results are in very good agreement with ED. This highlights that the stochastic formula for $\langle \hat{S}_i^z(t) \rangle$ in higher dimensions is the immediate generalization of the 1D result (21), where the products are extended over all the lattice sites. The same holds true for other local observables.

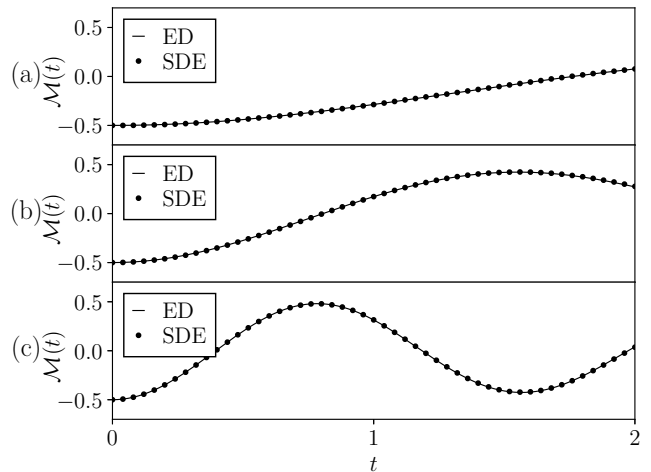


FIG. 5. Time-evolution of the magnetization $\mathcal{M}(t)$ for the 1D quantum Ising model following quantum quenches from the fully-polarized initial state $|\downarrow\rangle$ to different values of the final transverse field. (a) $\Gamma = 2\Gamma_c$, (b) $\Gamma = 4\Gamma_c$, (c) $\Gamma = 8\Gamma_c$. The SDE results (filled circles) computed from (a) 2×10^5 (b) 3×10^5 and (c) 4×10^5 trajectories, are in good agreement with ED (solid line) for $N = 3$ spins.

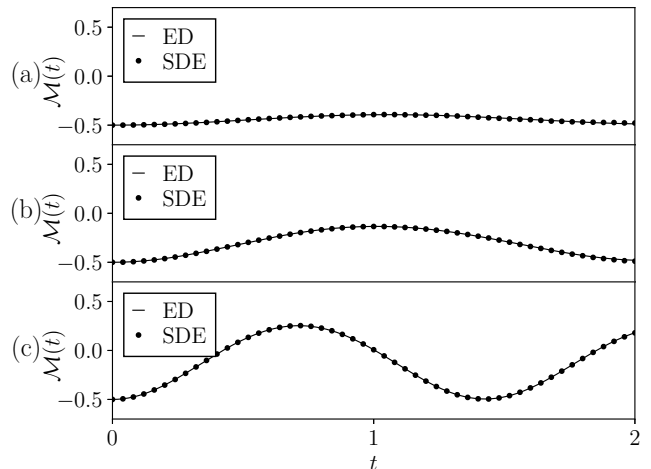


FIG. 6. Time-evolution of $\mathcal{M}(t)$ for the 1D quantum Ising model with an integrability-breaking longitudinal field $h = 2J$. We consider quantum quenches from the fully-polarized initial state $|\downarrow\rangle$ to (a) $\Gamma = J$, (b) $\Gamma = 2J$, and (c) $\Gamma = 4J$. The SDE results (filled circles) computed from (a) 5×10^5 (b) 2×10^5 and (c) 6×10^5 trajectories are in good agreement with ED (solid line) for $N = 3$ spins.

V. DYNAMICS OF THE DISENTANGLING VARIABLES

A notable feature of the stochastic approach to quantum spin systems is that it allows the derivation of exact stochastic formulae such as equations (19) and (21). In this framework, time-dependent quantum expectation values are obtained by averaging explicit functions of the

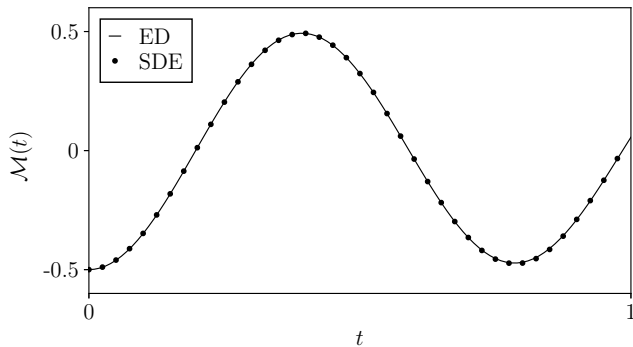


FIG. 7. Time-evolution of $\mathcal{M}(t)$ for a 2×3 site quantum Ising model following a quantum quench from the fully-polarized initial state $|\Downarrow\rangle$ to $\Gamma = 8J$. The SDE results (filled circles) obtained from 5×10^5 trajectories, are in very good agreement with ED (solid line). Less than 1% of the trajectories were found to be divergent at the stopping time.

classical stochastic variables, $\xi_i^a(t)$. It is therefore interesting to investigate to what extent the quantum dynamics is reflected in these classical variables.

A. Distributions of the Classical Variables

As we discussed in Section IV A, the stochastic formula for the Loschmidt amplitude has a particularly simple form for quantum quenches starting in the fully-polarized initial state $|\Downarrow\rangle$. In this case $A(t)$ can be written as [34]

$$A(t) = \langle e^{-\frac{N}{2}\chi^z(t)} \rangle_\phi, \quad (35)$$

where we define the site-averaged variables $\chi^a(t) \equiv N^{-1} \sum_i \xi_i^a(t)$. It is readily seen that the Loschmidt amplitude is directly determined by the statistical properties of $\chi^z(t)$. In particular, the functional form of (35) suggests that the peaks in $\lambda(t) \equiv -N^{-1} \log |A(t)|^2$ occur in close proximity to (although not necessarily coincident with) the peaks in the distribution of $\chi^z(t)$, and its classical average $\langle \chi^z(t) \rangle_\phi$ [34]. In Fig. 8(a) we show the time-evolution of the latter, which indeed exhibits maxima in the vicinity of the Loschmidt peaks, and has little dependence on system size. In addition, the turning points of $\langle \chi^z(t) \rangle_\phi$ coincide with the zeros of $\langle \chi^+(t) \rangle_\phi$ due to the exact relation $i\langle \dot{\chi}^z(t) \rangle_\phi = \Gamma \langle \chi^+(t) \rangle_\phi$, which follows from the Ising SDE in Eq. (26b) [34]. In general, it is important to stress that the average of the exponential in (35) is *not* the exponential of the average, $-N \langle \chi^z(t) \rangle_\phi / 2$. As such, the turning points of $\langle \chi^z(t) \rangle_\phi$ are not in general located at the exact positions of the Loschmidt peaks. In Fig. 9 we show the comparison between the turning points of $\langle \chi^z(t) \rangle_\phi$, or equivalently the zeros of $\langle \chi^+(t) \rangle_\phi$, and the Loschmidt peak times obtained via ED, for different quantum quenches. It is evident that these quantities are in excellent quantitative agreement for quenches with $\Gamma \gg \Gamma_c$, but differ for $\Gamma \sim \Gamma_c$. This can be understood from the Ising SDEs in (26). In the limit $\Gamma \rightarrow \infty$

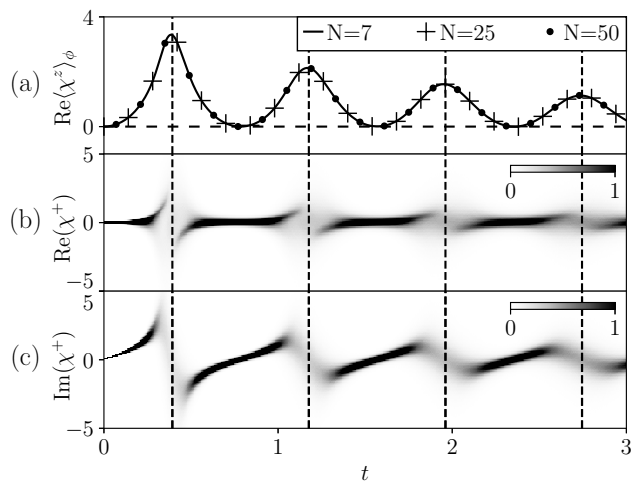


FIG. 8. Time-evolution of the disentangling variables in the 1D quantum Ising model following a quantum quench from the fully-polarized initial state $|\Downarrow\rangle$ to $\Gamma = 16\Gamma_c$. (a) Dynamics of $\text{Re}(\chi^z(t))_\phi$ for $N = 7, 25, 50$ spins showing maxima in the vicinity of the Loschmidt peak times. The latter are obtained by ED (dashed lines). Dynamics of the distribution of (b) $\text{Re} \chi^+(t)$ and (c) $\text{Im} \chi^+(t)$ for $N = 7$ spins showing signatures of the DQPTs.

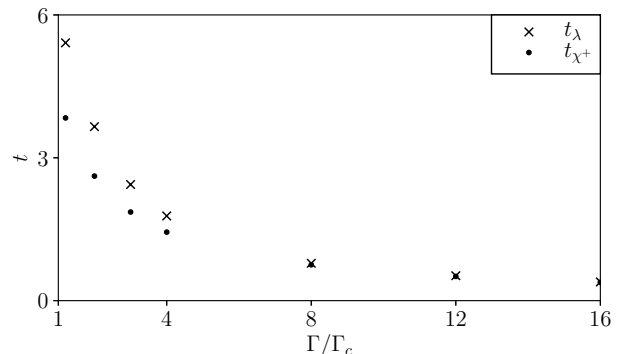


FIG. 9. Comparison of the time t_λ of the first Loschmidt peak obtained by ED (crosses) and the time t_{χ^+} of the zeros of $\text{Im}(\chi^+(t))_\phi$ (dots) for the 1D quantum Ising model with $N = 7$ sites. The data correspond to quantum quenches from the fully-polarized initial state $|\Downarrow\rangle$ to different values of Γ . In the limit of large Γ the results coincide, but for small Γ , the results of ED differ from those given by the approximation $\text{Im}(\chi^+(t))_\phi = 0$. Note that for $\Gamma < \Gamma_c$ (not shown), there are no DQPTs for $N \rightarrow \infty$. However, zeros of $\text{Im}(\chi^+(t))_\phi$ persist for $\Gamma < \Gamma_c$; these get pushed to later times as Γ decreases.

the equations become deterministic and the average of the exponential in (35) is equal to the exponential of the average; away from this limit, this is not the case. Nonetheless, the exact formula (35) still applies, and its predictions are in good agreement with ED.

Signatures of the DQPTs can also be seen in the distributions of the classical variables, which show marked features and enhanced broadening in their vicinity as shown in Figs 8(b) and (c). In particular, the distri-

bution of $\text{Re } \chi^z(t)$ is approximately Gaussian away from the DQPTs, but is non-Gaussian in their proximity, as illustrated in Fig. 10(a).

The departures from Gaussianity can be quantified by using the Kolmogorov–Smirnov (KS) test [51]. In this test, one considers the KS statistic D , which measures the deviation of the observed distribution $P(x)$ of a variable x from the best-fitting Gaussian distribution $P_G(x)$:

$$D \equiv \max_x |P(x) - P_G(x)|. \quad (36)$$

The aim of the test is to accept or reject the null hypothesis that the observed data come from a Gaussian distribution, to a given statistical significance. The statistical significance α is defined as the probability that the test rejects the null hypothesis when this is in fact true, i.e. the probability that the test fails to recognize a Gaussian distribution. The statistical significance α determines a critical value $D_c(\alpha)$ for which the null hypothesis is rejected with significance α when $D > D_c(\alpha)$. For a sufficiently large number of samples \mathcal{N} , the limiting distribution of D is given by [51]

$$P(\sqrt{\mathcal{N}}D > z) = 2 \sum_{r=1}^{\infty} (-1)^{r-1} e^{-2r^2 z^2}. \quad (37)$$

The critical value $D_c(\alpha)$, for a given α and number of samples \mathcal{N} , is then given by $D_c(\alpha) = z_c(\alpha)/\sqrt{\mathcal{N}}$, where $z_c(\alpha)$ is determined by solving $P(\sqrt{\mathcal{N}}D > z_c) = \alpha$.

To analyze the distribution of $\text{Re } \chi^z(t)$, we evaluate (36) with $x = \text{Re } \chi^z(t)$. The results of the KS test are shown in the inset of Fig. 10(a). The null hypothesis is rejected at the $\alpha = 5\%$ significance level in the shaded region surrounding the DQPT, indicating that the distribution of $\text{Re } \chi^z(t)$ is non-Gaussian in this region. This behavior persists for different system sizes, with the distributions becoming narrower as N increases, as shown in Fig. 10(b).

B. Bounds

The stochastic approach also enables one to derive bounds on the Loschmidt rate function, $\lambda(t) \equiv -N^{-1} \ln |A(t)|^2$, where $A(t) = \langle f(\chi(t)) \rangle_\phi$ and the function $f(\chi(t))$ depends on the initial conditions. Using the fact that $|\langle f(\chi(t)) \rangle_\phi| \leq \langle |f(\chi(t))| \rangle_\phi$ one immediately obtains $\lambda(t) \geq \lambda_b(t)$ where

$$\lambda_b(t) \equiv -\frac{2}{N} \ln \langle |f(\chi(t))| \rangle_\phi. \quad (38)$$

This is confirmed in Fig. 11(a), where we consider quenches from the fully-polarized initial state $|\Downarrow\rangle$, corresponding to $f(\chi(t)) = e^{-N\chi^z(t)/2}$. Application of Jensen’s inequality [52] in this case also shows that

$$\text{Re} \langle \chi^z(t) \rangle_\phi = -\frac{2}{N} \ln \langle |e^{-\frac{N}{2}\chi^z(t)}| \rangle_\phi \geq \lambda_b(t), \quad (39)$$

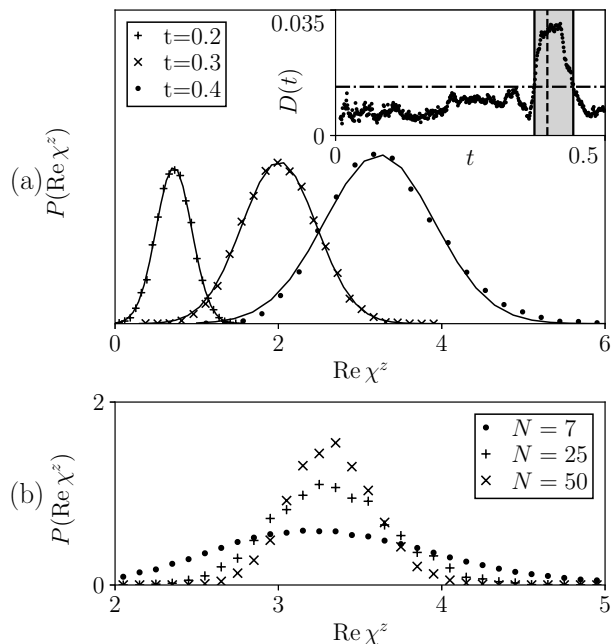


FIG. 10. (a) Time-evolution of the distribution of $\text{Re } \chi^z(t)$ for the 1D quantum Ising model with $N = 7$ spins. The data correspond to a quantum quench from the fully-polarized initial state $|\Downarrow\rangle$ with $\Gamma = 0$ to $\Gamma = 16\Gamma_c$, at times $t = 0.2$ (plus signs), $t = 0.3$ (crosses) and $t = 0.4$ (dots). We employ different normalizations for $P(\text{Re } \chi^z(t))$ at different t for ease of visualization. The distribution broadens on approaching the Loschmidt peak at $t = 0.39$, and narrows afterwards. The distribution is approximately Gaussian away from the Loschmidt peaks, as indicated by the Gaussian fits (solid lines), but is non-Gaussian in their vicinity. Inset: Time-evolution of the KS statistic $D(t)$ on passing through the first Loschmidt peak. We compare the value of $D(t)$ to the critical value of $D_c(\alpha)$ corresponding to the chosen significance of $\alpha = 5\%$ (dashed-dotted line). When $D > D_c(\alpha)$, the distribution can be regarded as non-Gaussian. This is observed in the shaded region near the DQPT, whose position is indicated by the dashed vertical line. (b) Variation of the distribution of $\text{Re } \chi^z(t)$ at $t = 0.39$ with increasing system size N . The distribution becomes more sharply peaked as N increases.

as confirmed in Fig. 11(b). As $\Gamma \rightarrow \infty$, the three quantities $\lambda(t)$, $\lambda_b(t)$ and $\text{Re} \langle \chi^z(t) \rangle_\phi$ all approach the non-interacting result, given in Eq. (G10b) in Appendix G. In this limit, as mentioned above, the SDEs (26) become purely deterministic and it is possible to replace the average of the exponential in Eq. (35) with the exponential of the average. As such, $\lambda(t)$ approaches $\text{Re} \langle \chi^z(t) \rangle_\phi$, in conformity with Fig. 8(a).

C. Correlations of the Classical Variables

The presence of DQPTs is also reflected in the correlation functions of the disentangling variables. To see this, it is convenient to define the site-averaged connected

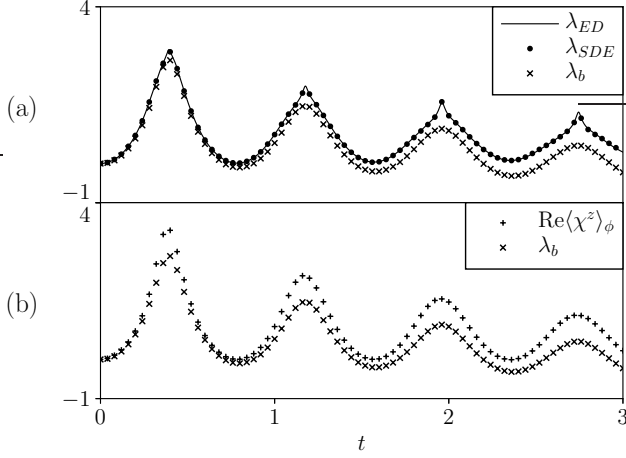


FIG. 11. (a) Time-dependent lower bound $\lambda_b(t)$ (crosses) on the Loschmidt rate function following a quantum quench in the 1D quantum Ising model from $\Gamma = 0$ to $\Gamma = 16\Gamma_c$. The data correspond to the solution of the Ising SDEs (filled circles), ED (solid line) and Eq. (38) with $f(\chi(t)) = e^{-N\chi^z(t)/2}$ (crosses) for an $N = 7$ site system. (b) The approximation to the Loschmidt rate function $\text{Re}\langle\chi^z(t)\rangle_\phi$ is also bounded by $\lambda_b(t)$. For large values of Γ , $\lambda(t)$, $\text{Re}\langle\chi^z(t)\rangle_\phi$ and $\lambda_b(t)$ coincide.

correlation function

$$\mathcal{C}_n^{ab}(t) \equiv \frac{1}{N} \sum_{i=1}^N (\langle \xi_i^a(t) \xi_{i+n}^b(t) \rangle_\phi - \langle \xi_i^a(t) \rangle \langle \xi_{i+n}^b(t) \rangle_\phi), \quad (40)$$

where n indicates the separation between the two sites. As can be seen in Fig. 12(a), $\text{Re} \mathcal{C}_1^{zz}(t)$ decreases smoothly over time, but $\text{Im} \mathcal{C}_1^{zz}(t)$ exhibits oscillations within an increasing envelope. In particular, $\text{Im} \mathcal{C}_1^{zz}(t)$ exhibits zeros in the vicinity of the Loschmidt peaks. Likewise, the second-neighbor correlation function $\text{Re} \mathcal{C}_2^{zz}(t)$ decreases rapidly in the vicinity of the DQPTs, while $\text{Im} \mathcal{C}_2^{zz}(t)$ remains zero for all t , as shown in Fig. 12(b); an analytical proof that $\text{Im} \mathcal{C}_n^{zz} = 0$ when $n \geq 2$ is provided in Appendix H. Fig. 13 shows an analogous analysis for $\mathcal{C}_n^{++}(t)$. It can be seen that first neighbor correlation functions take small values everywhere, except in the vicinity of the DQPTs where $\text{Im} \mathcal{C}_1^{++}(t)$ peaks; see Fig. 13(a). Likewise, the second neighbor correlation functions vanish on average for all times, but exhibit strong fluctuations in the vicinity of the Loschmidt peaks; see Fig. 13(b). The further neighbor correlation functions (not shown) are found to behave similarly to the second neighbor case, due to the nearest neighbor form of the \mathcal{J}_{ij} matrix under consideration. As prescribed by Eq. (16), the Ito drift is proportional to $\sum_k O_{ik} O_{jk} = 2\mathcal{J}_{ij}$, which is only non-zero when $j = i \pm 1$. As a result, the first neighbor correlation functions $\mathcal{C}_1^{zz}(t)$ and $\mathcal{C}_1^{++}(t)$ are qualitatively different from their further neighbor counterparts. In Appendix H, we provide further information on the moments of the disentangling variables, explicitly

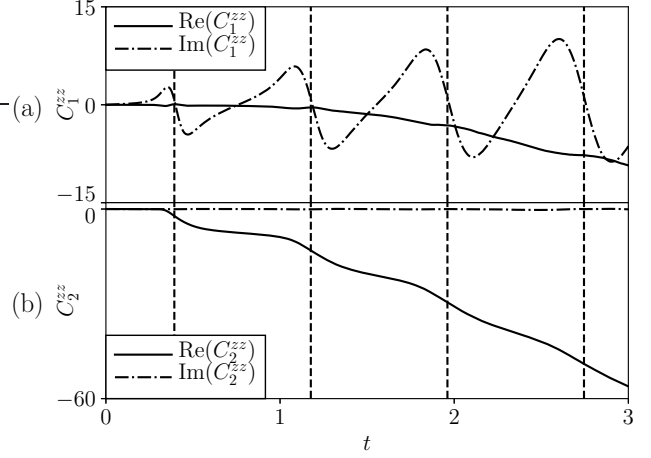


FIG. 12. Time-dependent connected correlation functions of the disentangling variables ξ_i^z following a quantum quench in the 1D quantum Ising model from $\Gamma = 0$ to $\Gamma = 16\Gamma_c$. (a) The first neighbor correlation function $\mathcal{C}_1^{zz}(t)$ has a monotonically decreasing real part and an oscillating imaginary part, with zeros occurring in the vicinity of the Loschmidt peaks (dashed lines, obtained from ED). (b) The second neighbor correlation function $\mathcal{C}_2^{zz}(t)$ has a vanishing imaginary part, but the real part decreases monotonically. The latter exhibits steeper gradients in the vicinity of the Loschmidt peaks.

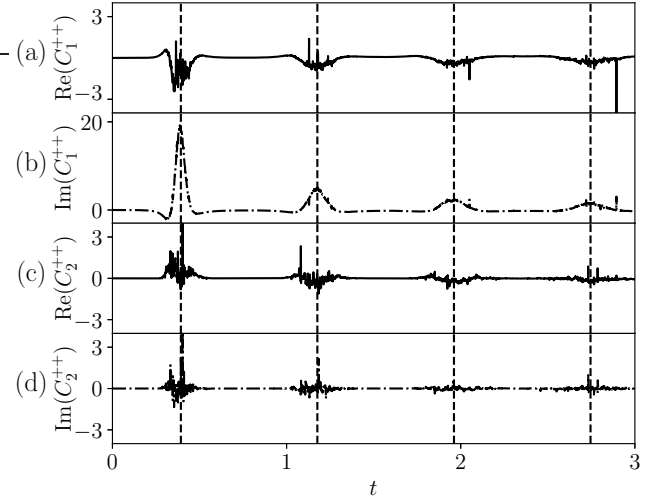


FIG. 13. Time-dependent connected correlation functions of the disentangling variables ξ_i^+ following a quantum quench in the 1D quantum Ising model from $\Gamma = 0$ to $\Gamma = 16\Gamma_c$. (a-b) The first neighbor correlation functions are small except in the vicinity of the Loschmidt peaks (dashed lines), when their imaginary part exhibits a sharp peak. (c-d) The second neighbor correlation functions vanish away from the Loschmidt peaks, but show enhanced fluctuations as the peak times are approached.

identifying a set of averages which vanish at all times.

VI. FLUCTUATIONS

As we have discussed above, the statistical properties of the disentangling variables play a central role in the stochastic approach to quantum spin systems. They provide access to time-dependent quantum expectation values and exhibit notable signatures in the vicinity of DQPTs. As we will discuss now, the fluctuations in the disentangling variables also provide insights into the current limitations of the stochastic approach. From a numerical perspective, the two main sources of error arise from the non-zero discretization time-step Δt , and the finite number of samples \mathcal{N} . The former is relatively benign for short timescales, but eventually leads to divergences in the stochastic variables at late times [43, 47]. This effect is more pronounced in the presence of large transverse fields Γ , and can be mitigated by reducing the time-step Δt . The latter is more important and arises from performing stochastic averages over a finite number of samples \mathcal{N} . For a quantum observable $\langle \hat{O}(t) \rangle$ corresponding to a stochastic function $f(\xi(t))$, as defined by (14), the formally exact expression is approximated by

$$\langle \hat{O}(t) \rangle \approx \frac{1}{\mathcal{N}} \sum_{r=1}^{\mathcal{N}} f_r(t) \equiv S_{\mathcal{N}}(t), \quad (41)$$

where $f_r(t)$ is the value of $f(t) = f(\xi(t))$ for a given realization r of the stochastic process. In the limit $\mathcal{N} \rightarrow \infty$, the central limit theorem implies that the sample average $S_{\mathcal{N}}(t)$ is Gaussian distributed, even if the individual $f_r(t)$ are not, provided that $f(t)$ has finite variance. The resulting Gaussian distribution has mean $\langle f(t) \rangle$, and standard deviation $\sigma_{\mathcal{N}}(t) = \sigma(t)/\sqrt{\mathcal{N}}$, where $\sigma(t)$ is the standard deviation of $f(t)$. The fluctuations in $S_{\mathcal{N}}(t)$ obtained by sampling the SDEs are therefore proportional to $\sigma(t)$; the value of $\sigma(t)$ thus determines the number of simulations required to achieve a given accuracy.

In order to quantify the growth of fluctuations it is instructive to consider the Loschmidt amplitude $A(t)$ given by (28), for quenches starting in the fully-polarized initial state $|\Downarrow\rangle$. Since the Loschmidt amplitude is exponentially suppressed with increasing system size, it is convenient to consider the strength of the fluctuations relative to the mean, using $\tilde{\sigma}(t) = \sigma(t)/|\langle f(t) \rangle|$. In the classical limit where $\Gamma = 0$, one can show that $|\langle f(t) \rangle| = 1$, so that $\tilde{\sigma}(t) = \sigma(t)$; see Appendix G. In this case

$$\tilde{\sigma}(t) = e^{\frac{JNt}{2}} - 1, \quad (42)$$

which exhibits exponential growth with time t and system size N according to $\tilde{\sigma}(t) \sim e^{JNt/2}$. In Fig. 14 we confirm this dependence numerically for quenches in the 1D quantum Ising model. A similar exponential growth of fluctuations is also observed for $\Gamma < \Gamma_c$, as shown in Fig. 14. In the regime $\Gamma > \Gamma_c$, enhanced fluctuations

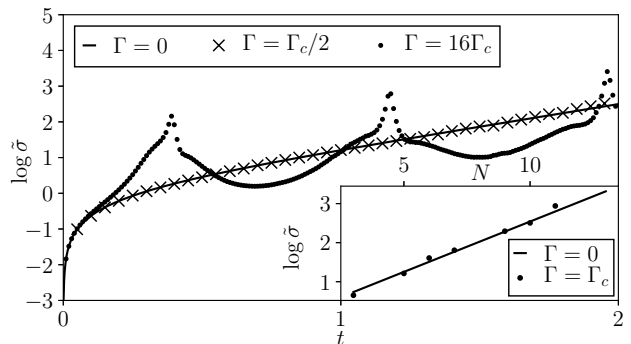


FIG. 14. Growth of fluctuations in the stochastic approach. (a) Time-evolution of the normalized standard deviation $\tilde{\sigma}(t)$ as defined in the text, for the Loschmidt amplitude $A(t)$. We consider quantum quenches in the 1D quantum Ising model with $N = 5$ from the fully-polarized initial state $|\Downarrow\rangle$ state to different values of Γ . The solid line shows the analytical result for the classical case $\Gamma = 0$, corresponding to exponential growth with t and N . For $\Gamma > \Gamma_c$, stronger fluctuations become visible in the vicinity of the Loschmidt peaks, but the overall growth is consistent with the classical case. Inset: growth of fluctuations with increasing N , for fixed Γ and $t = 1$. The results are consistent with exponential growth.

appear in the vicinity of the Loschmidt peaks, but the overall growth of fluctuations mirrors that in (42). Similar behavior is also observed for other observables and for different initial conditions. In the case of local observables, the presence of two time-evolution operators in Eq. (20) translates to an extra factor of 2 in the exponent, as shown in Appendix G for the magnetization. The exponential growth of fluctuations for large system sizes and long times ultimately limits the stochastic approach in its current form. As the fluctuations in $\tilde{\sigma}(t)$ increase, an increasing number of runs is required for the sample mean $S_{\mathcal{N}}(t)$ to converge to $\langle f(t) \rangle$. This is consistent with our numerical observations, as illustrated in Figs 15 and 16. The simulations typically breakdown at a characteristic time $t_b \sim 1/NJ$, when the variance of the spatially summed and time-integrated HS fields is of order unity; this can also be seen directly from Eq. (42).

VII. COMPUTATIONAL COST

A notable feature of the stochastic approach to quantum spin systems is that the numerical solution of the SDEs is intrinsically parallelizable; the stochastic averages are performed over independent trajectories and the number of stochastic variables scales linearly in N , due to the HS decoupling of the interactions. The simulation time also scales linearly with t and \mathcal{N} , and inversely with Δt . However, as t and N increase, the exponential growth in the fluctuations requires increasing \mathcal{N} ; this necessitates much longer simulation times than suggested by the naïve linear scaling. Eventually, the averages ob-

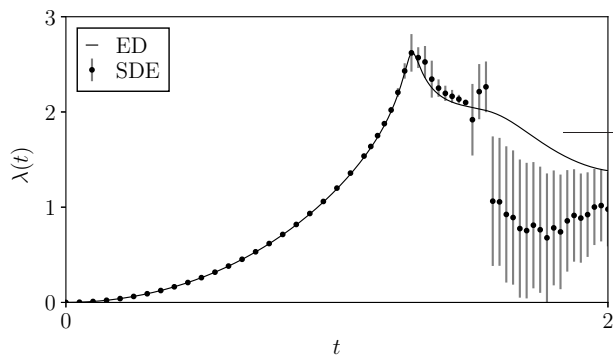


FIG. 15. Loschmidt rate function $\lambda(t)$ for the same quantum quench considered in Fig. 4, but extending the simulation time. As can be seen from the vertical bars (light grey), for $t \gtrsim 1.3$ strong fluctuations in the disentangling variables hamper the convergence of the stochastic averages (filled dots) to the results obtained by ED (solid line).

tained from a given number of trajectories fail to converge to the required quantum expectation values, due to the increasing variance of the stochastic variables; see Figs 14, 15 and 16. In the case of the Loschmidt amplitude, each batch of $\mathcal{N} = 10^5$ simulations with $\Delta t = 10^{-5}$ takes approximately 1 hour on 96 cores, per unit interval of time, and per lattice site, i.e. the data in Fig. 1 correspond to approximately 14 hours of simulation time. Local expectation values take a factor of two longer due to the presence of two sets of disentangling variables. From a numerical perspective, this is clearly inferior to ED for small system sizes. However, for larger system sizes, the stochastic approach may offer some advantages as the number of stochastic variables scales linearly in N . In contrast to ED, one also avoids having to store an exponentially large matrix in memory. However, this advantage is offset to some extent as the breakdown time $t_b \sim 1/NJ$ decreases with increasing system size due to the growth of stochastic fluctuations, i.e. there is a trade off between increasing the system size N and the timescale that can be addressed. We also observe slower convergence in the regions where the fluctuations are strongest; see Figs 14 and 16. This could perhaps be mitigated through the use of enhanced sampling techniques. Nonetheless, in spite of these numerical and computational challenges, the stochastic approach offers a new set of tools for describing non-equilibrium quantum spin systems. This includes exact stochastic formulae with wide applicability, which hold in arbitrary dimensions and in the absence of integrability. The stochastic approach also provides direct links between quantum and classical dynamics, enabling the transfer of ideas between different domains of non-equilibrium science.

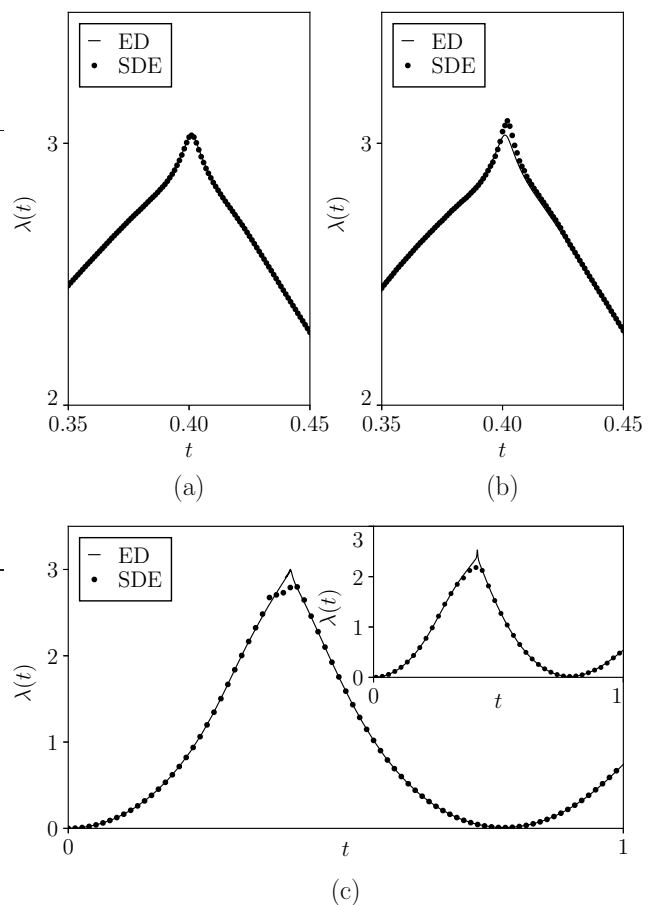


FIG. 16. (a) Close-up of the first Loschmidt peak for the 1D quantum Ising model with $N = 14$ spins following a quantum quench from $\Gamma = 0$ to $\Gamma = 16\Gamma_c$. Using $n = 3 \times 10^6$ independent trajectories we reproduce the ED result for $\lambda(t)$. (b) Results for the same quench, but with $n = 3 \times 10^5$ trajectories. For this smaller number of simulations, $\lambda(t)$ converges to the ED result, except in the immediate vicinity of the peak. (c) Loschmidt rate function for the quench in panel (a), but for $N = 21$ spins. For $n = 5 \times 10^6$ simulations, $\lambda(t)$ at the peak has not yet converged to the ED value. This is due to the enhanced fluctuations in the disentangling variables ξ_i^z in the vicinity of the peaks, which grow with N ; see Fig. 14. Near the peak, the sampling is insufficient to reproduce the ED result. However, in all other regions of the plot, including times beyond the peak, the result obtained from the SDEs is in good agreement with ED. This highlights that the method is formally exact, but that sampling is important in order to achieve convergence. Inset: analogous results for a 5×5 quantum Ising model, corresponding to the upper limit for comparison with ED. The system was initialized in the fully-polarized state $|\Downarrow\rangle$ and time-evolved with $\Gamma = 8J$. The results for $n = 4 \times 10^7$ are similar to those in panel (c): the SDE results are in good agreement with ED before and after the peak, but the sampling is insufficient to resolve the peak.

VIII. CONCLUSION

In this work we have investigated a stochastic approach to non-equilibrium quantum spin systems based on an exact mapping of quantum dynamics to classical SDEs. We have provided exact stochastic formulae for a variety of quantum observables, with broad applicability for spin-1/2 systems. We have also outlined the general approach to express other observables in this framework. We have illustrated the method in the context of the one- and two-dimensional quantum Ising model, highlighting the role of the classical stochastic variables and their relation to dynamical quantum phase transitions. We have also explored the growth of fluctuations in the stochastic approach, discussing their scaling with time and system size, including details of the numerical aspects of the current implementation of the method. There are many directions for future research, including the development of improved sampling methods as well as further exploration of the correspondence between the quantum and classical dynamics.

We acknowledge helpful conversations with Samuel

Begg, John Chalker, Andrew Green, Vladimir Gritsev, Lev Kantorovich and Austen Lamacraft. MJB is very grateful to John Chalker for early discussions on the Hubbard–Stratonovich and stochastic approaches to quantum dynamics. BD is a Royal Society Leverhulme Trust Senior Research Fellow, ref. SRF\R1\180103. SDN acknowledges funding from the Institute of Science and Technology (IST) Austria, and from the European Union’s Horizon 2020 research and innovation programme under the Marie Skłodowska-Curie Grant Agreement No. 754411. SDN also acknowledges funding from the EPSRC Centre for Doctoral Training in Cross-Disciplinary Approaches to Non-Equilibrium Systems (CANES) under grant EP/L015854/1. MJB, BD and SDN thank the Centre for Non-Equilibrium Science (CNES) and the Thomas Young Centre (TYC). We are grateful to the UK Materials and Molecular Modelling Hub for computational resources, which is partially funded by EPSRC (EP/P020194/1). We acknowledge computer time on the Rosalind High Performance Computer Cluster.

-
- [1] T. Kinoshita, T. Wenger, and D. S. Weiss, *Nature* **440**, 900 (2006).
- [2] C. Weitenberg, M. Endres, J. F. Sherson, M. Cheneau, P. Schausz, T. Fukuhara, I. Bloch, and S. Kuhr, *Nature* **471**, 319 (2011).
- [3] R. Blatt and C. F. Roos, *Nature Phys.* **8**, 277 (2012).
- [4] T. Langen, S. Erne, R. Geiger, B. Rauer, T. Schweigler, M. Kuhnert, W. Rohringer, I. E. Mazets, T. Gasenzer, and J. Schmiedmayer, *Science* **348**, 207 (2015).
- [5] T. Langen, R. Geiger, and J. Schmiedmayer, *Annu. Rev. Condens. Matter Phys.* **6**, 201 (2015).
- [6] C. Gross and I. Bloch, *Science* **357**, 995 (2017).
- [7] A. Polkovnikov, K. Sengupta, A. Silva, and M. Vengalattore, *Rev. Mod. Phys.* **83**, 863 (2011).
- [8] J. Eisert, M. Friesdorf, and C. Gogolin, *Nature Phys.* **11**, 124 (2015).
- [9] P. Calabrese and J. Cardy, *J. Stat. Mech. Theor. Exp.* **2005**, P04010 (2005).
- [10] P. Calabrese and J. Cardy, *Phys. Rev. Lett.* **96**, 136801 (2006).
- [11] P. Calabrese, F. H. L. Essler, and G. Mussardo, *J. Stat. Mech. Theor. Exp.* **2016**, 064001 (2016).
- [12] M. Rigol, A. Muramatsu, and M. Olshanii, *Phys. Rev. A* **74**, 053616 (2006).
- [13] M. Rigol, V. Dunjko, V. Yurovsky, and M. Olshanii, *Phys. Rev. Lett.* **98**, 050405 (2007).
- [14] M. Rigol, V. Dunjko, and M. Olshanii, *Nature* **452**, 854 (2008).
- [15] J.-S. Caux and F. H. L. Essler, *Phys. Rev. Lett.* **110**, 257203 (2013).
- [16] J.-S. Caux, *J. Stat. Mech. Theor. Exp.* **2016**, 064006 (2016).
- [17] M. J. Bhaseen, B. Doyon, A. Lucas, and K. Schalm, *Nature Phys.* **11**, 509 (2015).
- [18] B. Doyon, A. Lucas, K. Schalm, and M. J. Bhaseen, *J. Phys. A: Math. Theor.* **48**, 095002 (2015).
- [19] D. Bernard and B. Doyon, *J. Stat. Mech. Theor. Exp.* **2016**, 064005 (2016).
- [20] O. A. Castro-Alvaredo, B. Doyon, and T. Yoshimura, *Phys. Rev. X* **6**, 041065 (2016).
- [21] B. Bertini, M. Collura, J. De Nardis, and M. Fagotti, *Phys. Rev. Lett.* **117**, 207201 (2016).
- [22] M. A. Cazalilla and J. B. Marston, *Phys. Rev. Lett.* **88**, 256403 (2002).
- [23] G. Vidal, *Phys. Rev. Lett.* **91**, 147902 (2003).
- [24] G. Vidal, *Phys. Rev. Lett.* **93**, 040502 (2004).
- [25] S. R. White and A. E. Feiguin, *Phys. Rev. Lett.* **93**, 1 (2004).
- [26] J. J. García-Ripoll, *New J. Phys.* **8**, 305 (2006).
- [27] U. Schollwöck, *Ann. Phys. (N. Y.)* **326**, 96 (2011).
- [28] M. Heyl, A. Polkovnikov, and S. Kehrein, *Phys. Rev. Lett.* **110**, 135704 (2013).
- [29] M. Heyl, *Rep. Prog. Phys.* **81**, 054001 (2018).
- [30] P. Jurcevic, H. Shen, P. Hauke, C. Maier, T. Brydges, C. Hempel, B. P. Lanyon, M. Heyl, R. Blatt, and C. F. Roos, *Phys. Rev. Lett.* **119**, 080501 (2017).
- [31] P. M. Hogan and J. T. Chalker, *J. Phys. A: Math. Gen.* **37**, 11751 (2004).
- [32] V. Galitski, *Phys. Rev. A* **84**, 012118 (2011).
- [33] M. Ringel and V. Gritsev, *Phys. Rev. A* **88**, 062105 (2013).
- [34] S. De Nicola, B. Doyon, and M. J. Bhaseen, *J. Phys. A: Math. Theor.* **52**, 05LT02 (2019).
- [35] A. Polkovnikov, *Ann. Phys. (N. Y.)* **325**, 1790 (2010).
- [36] R. Ng and E. S. Sørensen, *J. Phys. A Math. Theor.* **44**, 065305 (2011).
- [37] J. Wurtz, A. Polkovnikov, and D. Sels, *Ann. Phys. (N. Y.)* **395**, 341 (2018).
- [38] R. L. Stratonovich, *Sov. Phys. Dokl.* **2**, 416 (1957).
- [39] J. Hubbard, *Phys. Rev. Lett.* **3**, 77 (1959).

- [40] H. F. Trotter, Proc. Amer. Math. Soc. **10**, 545 (1959).
 [41] J. Wei and E. Norman, J. Math. Phys. **4**, 575 (1963).
 [42] I. Kolokolov, Phys. Lett. A **114**, 99 (1986).
 [43] P. E. Kloeden and E. Platen, *Numerical Solution of Stochastic Differential Equations* (Springer, 1992).
 [44] A. LeClair, G. Mussardo, H. Saleur, and S. Skorik, Nucl. Phys. B **453**, 581 (1995).
 [45] N. Kitanine, J. M. Maillet, N. A. Slavnov, and V. Terras, (2005), arXiv:0505006.
 [46] For system sizes N that are multiples of 4, we add a constant diagonal shift to the interaction matrix \mathcal{J} in order to make it diagonalizable; see Appendix B.
 [47] M. Hutzenthaler, A. Jentzen, and P. E. Kloeden, Proc. R. Soc. A Math. Phys. Eng. Sci. **467**, 1563 (2011).
 [48] P. Weinberg and M. Bukov, SciPost Phys. **2**, 003 (2017).
 [49] P. Pfeuty and R. J. Elliott, J. Phys. C Solid State Phys. **4**, 2370 (1971).
 [50] M. S. L. du Croo de Jongh and J. M. J. van Leeuwen, Phys. Rev. B **57**, 8494 (1998).
 [51] F. James, *Statistical Methods in Experimental Physics* (World Scientific, 2006).

- [52] G. H. Hardy, J. E. Littlewood, and G. Polya, *Inequalities* (Cambridge University Press, 1934).
 [53] K. Ito, Proc. Imp. Acad. **20**, 519 (1944).

Appendix A: Hubbard–Stratonovich Decoupling of the Time-Evolution Operator

In Section II A we gave a brief overview of the Hubbard–Stratonovich decoupling of the time-evolution operator $\hat{U}(t) = \mathbb{T}e^{-i \int_0^t \hat{H} dt'}$, where

$$\hat{H} = - \sum_{ijab} \mathcal{J}_{ij}^{ab} \hat{S}_i^a \hat{S}_j^b - \sum_{ia} h_i^a \hat{S}_i^a, \quad (\text{A1})$$

is a generic Heisenberg model. Here we provide some of the technical details involved in this procedure. Trotter-slicing the time-ordered exponential in $\hat{U}(t)$ one obtains

$$\hat{U}(t) = \mathbb{T} \exp \left(-i \int_0^t dt' \hat{H}(t') \right) = \mathbb{T} \lim_{n \rightarrow \infty} \prod_{m=1}^n \exp \left(i \Delta t \sum_{ijab} \mathcal{J}_{ij}^{ab} (m \Delta t) \hat{S}_i^a \hat{S}_j^b + i \Delta t \sum_{ja} h_j^a (m \Delta t) \hat{S}_j^a \right), \quad (\text{A2})$$

where $\Delta t \equiv t/n$. Performing the Hubbard–Stratonovich

transformation at each time slice yields

$$e^{i \Delta t \sum_{ijab} \mathcal{J}_{ij}^{ab} \hat{S}_i^a \hat{S}_j^b} = \mathcal{C} \int \prod_{ia} (d\varphi_i^a) e^{-\frac{1}{4} \Delta t \sum_{ijab} (\mathcal{J}^{-1})_{ij}^{ab} \varphi_i^a \varphi_j^b + \sqrt{i} \Delta t \sum_{ja} \varphi_j^a \hat{S}_j^a}, \quad (\text{A3})$$

where \mathcal{C} is a normalization constant and φ_i^a are complex scalar fields chosen in such a way as to ensure convergence of the integral in (A3); see the discussion following Eq. (A8) below. In order to show that Eq. (A3) holds for spin operators \hat{S}_i^a , it is convenient to introduce multicomponent indices $\alpha = \{i, a\}$ so that e.g. $\mathcal{J}_{ij}^{ab} \equiv \mathcal{J}_{\alpha\beta}$:

$$e^{i \Delta t \sum_{ijab} \mathcal{J}_{ij}^{ab} \hat{S}_i^a \hat{S}_j^b} \equiv e^{i \Delta t \sum_{\alpha\beta} \mathcal{J}_{\alpha\beta} \hat{S}_\alpha \hat{S}_\beta}. \quad (\text{A4})$$

For simplicity, we assume that the matrix $\mathcal{J}_{\alpha\beta}$ is symmetric, as it can always be redefined so that this is true. Then, $\mathcal{J}_{\alpha\beta}$ can be diagonalized as follows. We define the matrix Q whose columns are the orthonormal eigenvectors $e^{(\alpha)}$ of \mathcal{J} , so that $Q_{\alpha\beta} = e_{\alpha}^{(\beta)}$:

$$Q \equiv \begin{pmatrix} e^{(1)} & \dots & e^{(3N)} \\ \downarrow & \dots & \downarrow \end{pmatrix}. \quad (\text{A5})$$

This is an orthogonal matrix satisfying $QQ^T = Q^TQ = \mathbb{1}$. We also define the diagonal matrix $D \equiv \text{diag}(\lambda_1, \dots, \lambda_{3N})$, whose elements are the (real-valued)

eigenvalues of \mathcal{J} , arranged in the same order as the columns of Q , so that $Q^T \mathcal{J} Q = D$. Using these, Eq. (A4) can be written as

$$e^{i \Delta t \sum_{\alpha\beta} \mathcal{J}_{\alpha\beta} \hat{S}_\alpha \hat{S}_\beta} = e^{i \Delta t \sum_{\alpha} \lambda_{\alpha} \hat{S}_{\alpha}^2}. \quad (\text{A6})$$

where we have defined the operators $\hat{S}_{\alpha} \equiv \sum_{\beta} (Q^T)_{\alpha\beta} \hat{S}_{\beta}$. For example, for the quantum Ising model (25) the \hat{S}_{α} are linear combinations of the \hat{S}_i^z operators at different sites. One can now factorize the infinitesimal exponentials in Eq. (A6) over α using

$$e^{i \Delta t \sum_{\alpha} \lambda_{\alpha} \hat{S}_{\alpha}^2} = \prod_{\alpha} e^{i \Delta t \lambda_{\alpha} \hat{S}_{\alpha}^2}, \quad (\text{A7})$$

where we neglect terms of order $(\Delta t)^2$ in the exponent. For each factor in Eq. (A7), one obtains

$$e^{i \Delta t \lambda_{\alpha} \hat{S}_{\alpha}^2} = C_{\alpha} \int d\bar{\varphi}_{\alpha} e^{-\frac{1}{4} \Delta t \lambda_{\alpha}^{-1} \bar{\varphi}_{\alpha}^2 + \sqrt{i} \Delta t \bar{\varphi}_{\alpha} \hat{S}_{\alpha}} \quad (\text{A8})$$

where C_{α} is a normalization constant. Since \hat{S}_{α} commutes with itself, the above Gaussian equality can be

proved by Taylor expansion of the integrand, where the integration over $\bar{\varphi}_\alpha$ is carried out along the real (imaginary) axis for all positive (negative) eigenvalues λ_α . Finally, by changing variables using $\bar{\varphi}_\alpha = \sum_\beta (Q^T)_{\alpha\beta} \varphi_\beta$, the operator identity (A3) is verified.

Appendix B: Diagonalization of the Noise Action

Following the application of the Hubbard–Stratonovich transformation, we define the *noise action* $S[\varphi]$ as

$$S[\varphi] \equiv \sum_{ijab} \int_0^t \frac{1}{4} (\mathcal{J}^{-1})_{ij}^{ab} \varphi_i^a(t') \varphi_j^b(t') dt'. \quad (\text{B1})$$

We want to perform a change of variables $\varphi_i^a = \sum_{jb} O_{ij}^{ab} \phi_j^b$ so that Eq. (B1) can be recast in the form

$$S[\phi] \equiv \sum_{ia} \int_0^t \frac{1}{2} \phi_i^a(t') \phi_i^a(t') dt'. \quad (\text{B2})$$

For a symmetric interaction matrix \mathcal{J}_{ij}^{ab} , one can always construct a matrix O_{ij}^{ab} that diagonalizes (B1). Using the matrices Q and D introduced in Appendix A, the matrix

$$O \equiv \sqrt{2} Q D^{1/2} \quad (\text{B3})$$

satisfies $O^T \mathcal{J}^{-1} O / 2 = \mathbb{1}$ and can thus be used to put the noise action in the desired form (B2). The matrix O also satisfies $OO^T = 2\mathcal{J}$, which is a useful relation when converting the SDEs between the Ito and Stratonovich conventions; see Appendix D. By writing O in terms of its real and imaginary parts O_R, O_I , one also obtains $O_R O_R^T - O_I O_I^T = \mathcal{J}$. Due to the definition (B3), where the matrix Q is real valued and the entries of the diagonal matrix $D^{1/2}$ are either purely real or purely imaginary, O has either purely real or purely imaginary columns. This implies that $O_I O_R^T = O_R O_I^T = 0$. We will use these properties of O_R and O_I in Appendix G. The definition of the matrix O is not unique and depends on the specific ordering of the eigenvalues in (A5). This construction breaks down if the interaction matrix has vanishing eigenvalues and cannot be inverted. This is relevant to the quantum Ising model (25) for example. In this case, the interaction matrix is given by

$$\mathcal{J}_{ij}^{ab} = \frac{J}{2} \delta_{az} \delta_{bz} (\delta_{ij+1} + \delta_{ij-1}) \equiv \delta_{az} \delta_{bz} \mathcal{J}_{ij}. \quad (\text{B4})$$

When the system size N is a multiple of 4, one of the eigenvalues of \mathcal{J} turns out to be zero. For spin-1/2 systems this can be avoided by including a shift proportional to the identity operator in the Hamiltonian. Using the fact that $\sum_i (S_i^z)^2 = \frac{N}{4} \mathbb{1}$, this may be achieved by adding a term $J_s \delta_{ij} \delta_{az} \delta_{bz}$ to the interaction matrix. For $J_s \neq 1$, \mathcal{J} becomes invertible. The corresponding time-evolution operator acquires a constant phase shift, which does not affect the computation of physical observables. However, with this modification, $\mathcal{J}_{ii} \neq 0$ and thus $(OO^T)_{ii} \neq 0$. This leads to a change in the stochastic equations of motion, as discussed in Appendix D.

Appendix C: Disentanglement Transformation

As we discussed in Section IIB, the stochastic time-evolution operator $\hat{U}_j^s(t)$ can be simplified by means of a *disentanglement transformation* [31–33]:

$$\hat{U}_j^s(t) \equiv \mathbb{T} e^{i \int_0^t \sum_a \Phi_j^a(t) \hat{S}_j^a} = e^{\xi_j^+(t) \hat{S}_j^+} e^{\xi_j^z(t) \hat{S}_j^z} e^{\xi_j^-(t) \hat{S}_j^-}, \quad (\text{C1})$$

where the explicit group parameterization eliminates the time-ordering operation. In order to obtain the evolution equations satisfied by the disentangling variables ξ_j^a [33], one may differentiate (C1) with respect to time. Right-multiplying the result by $(\hat{U}_j^s)^{-1}$ one obtains

$$(\partial_t \hat{U}_j^s) (\hat{U}_j^s)^{-1} = i \sum_a \Phi_j^a \hat{S}_j^a, \quad (\text{C2})$$

or, equivalently,

$$\sum_a \left(\partial_t \xi_j^a \frac{\partial \hat{U}_j^s}{\partial \xi_j^a} \right) (\hat{U}_j^s)^{-1} = i \sum_a \Phi_j^a \hat{S}_j^a. \quad (\text{C3})$$

For this equality to hold, the coefficients of \hat{S}_j^a on each side of Eq. (C3) must be equal. Considering each spin component $a \in \{+, z, -\}$ in turn, it may be verified that

$$\left(\frac{\partial \hat{U}_j^s}{\partial \xi_j^+} \right) (\hat{U}_j^s)^{-1} = \hat{S}_j^+. \quad (\text{C4})$$

Similarly,

$$\left(\frac{\partial \hat{U}_j^s}{\partial \xi_j^z} \right) (\hat{U}_j^s)^{-1} = \hat{S}_j^z - \xi_j^+ \hat{S}_j^+. \quad (\text{C5})$$

In deriving this expression we invoke Hadamard's lemma

$$e^{\hat{A}} \hat{B} e^{-\hat{A}} = \hat{B} + [\hat{A}, \hat{B}] + \frac{1}{2!} [\hat{A}, [\hat{A}, \hat{B}]] + \dots, \quad (\text{C6})$$

and the commutation relations of $su(2)$: $[\hat{S}^z, \hat{S}^+] = \hat{S}^+$, $[\hat{S}^z, \hat{S}^-] = -\hat{S}^-$, $[\hat{S}^+, \hat{S}^-] = 2\hat{S}^z$. Finally,

$$\left(\frac{\partial \hat{U}_j^s}{\partial \xi_j^-} \right) (\hat{U}_j^s)^{-1} = e^{-\xi_j^z} \left(\hat{S}_j^- + 2\xi_j^+ \hat{S}_j^z - \xi_j^{+2} \hat{S}_j^+ \right). \quad (\text{C7})$$

Equating the coefficients of each \hat{S}_j^a one obtains

$$i\Phi_j^+ = \dot{\xi}_j^+ - e^{-\xi_j^z} \xi_j^{+2} \dot{\xi}_j^- - \xi_j^+ \dot{\xi}_j^z, \quad (\text{C8a})$$

$$i\Phi_j^z = \dot{\xi}_j^z + 2\xi_j^+ e^{-\xi_j^z} \dot{\xi}_j^-, \quad (\text{C8b})$$

$$i\Phi_j^- = e^{-\xi_j^z} \dot{\xi}_j^-. \quad (\text{C8c})$$

Rearranging for $\dot{\xi}_j^a$ yields the SDEs [33]

$$-i\dot{\xi}_j^+ = \Phi_j^+ + \Phi_j^z \xi_j^+ - \Phi_j^- \xi_j^{+2}, \quad (\text{C9a})$$

$$-i\dot{\xi}_j^z = \Phi_j^z - 2\Phi_j^- \xi_j^+, \quad (\text{C9b})$$

$$-i\dot{\xi}_j^- = \Phi_j^- \exp \xi_j^z. \quad (\text{C9c})$$

Appendix D: Ito and Stratonovich Conventions

In order to consistently define a stochastic differential equation, it is necessary to specify a discretization convention [43]. These are distinguished by how the values of a function $\bar{f}(t_j)$ defined at discrete times $t_j \equiv j\Delta t$ are assigned from the values of its continuous counterpart $f(t)$. Different discretization schemes are parameterized by a constant α as

$$\bar{f}(t_j) = \alpha f(t_j) + (1 - \alpha)f(t_{j-1}), \quad 0 \leq \alpha \leq 1. \quad (\text{D1})$$

The choice $\alpha = 0$ gives the Ito convention $\bar{f}(t_j) = f(t_{j-1})$, while $\alpha = 1/2$ gives the Stratonovich convention. The latter corresponds to choosing $\bar{f}(t_j)$ as the average of the values of $f(t)$ at t_{j-1}, t_j . Since $[f(t_j) + f(t_{j-1})]/2 \approx f[(t_j + t_{j-1})/2]$, the Stratonovich convention is also known as the *mid-point* prescription. SDEs in the Stratonovich convention satisfy the rules of ordinary calculus. However, when working with Ito SDEs a specific calculus is required [43, 53]. If we interpret the disentangling equations (10) as SDEs, they are to be understood as initially expressed in the Stratonovich convention. This is the form which arises naturally in physical applications involving well-defined continuous processes, i.e. noise with a finite correlation time, in the limit of the correlation time going to zero. However, equations in the Ito convention are typically mathematically and computationally simpler to handle. It is therefore often convenient to translate Stratonovich SDEs into the Ito form. In the Stratonovich form, the SDE for the disentangling variables ξ_i^a , collectively represented as a vector ξ_S , can be written as

$$\frac{d\xi_S}{dt} = A_S(\xi_S, t) + B_S(\xi_S, t)\phi, \quad (\text{D2})$$

where ϕ is a vector composed of the stochastic variables ϕ_j^a , A_S is the drift vector and B_S is a matrix of diffusion coefficients. The corresponding SDE for the vector ξ in the Ito convention is given by

$$\frac{d\xi}{dt} = A(\xi, t) + B(\xi, t)\phi, \quad (\text{D3})$$

where

$$A = A_S + \frac{1}{2}(B^T \nabla_\xi)B^T, \quad (\text{D4a})$$

$$B = B_S. \quad (\text{D4b})$$

For the quantum Ising model (25), this modification only affects the Ito SDE (26a) for ξ_j^+ , which becomes

$$-i\dot{\xi}_j^+ = \frac{1}{2}\Gamma(1 - \xi_j^{+2}) + \frac{1}{2}\xi_j^+ \sum_k O_{jk} O_{jk} + \xi_j^+ \sum_k O_{jk} \phi_k / \sqrt{i}. \quad (\text{D5})$$

In many cases, the extra term $\xi_j^+ \sum_k O_{jk} O_{jk} / 2$ vanishes, since $OO^T = 2\mathcal{J}$ and the interaction matrix \mathcal{J} typically

has no diagonal elements. However, as discussed in Appendix B, for system sizes N that are multiples of 4 we add a diagonal constant shift to \mathcal{J} , in order to make it invertible. In this case, the SDE for ξ_j^+ takes the form (D5). This leads to different behavior for the classical variables, but does not affect the resulting physical observables.

Appendix E: Analytical Averaging of the Equations of Motion

As we discussed in Section II C, in principle it is possible to analytically average the SDEs governing the dynamics of physical observables. The expectation value of an observable \hat{O} following time-evolution from an initial state $|\psi_0\rangle$ can be expressed as

$$\langle \hat{O}(t) \rangle = \langle f(t) \rangle_{\phi, \tilde{\phi}}, \quad (\text{E1})$$

where

$$f(t) = \langle \psi_0 | [\hat{U}^s(\tilde{\xi}(t))]^\dagger \hat{O} \hat{U}^s(\xi(t)) | \psi_0 \rangle. \quad (\text{E2})$$

Here, $\hat{U}^s = \otimes_i \hat{U}_i^s$ and the two time-evolution operators depend on independent stochastic processes ϕ and $\tilde{\phi}$ via $\xi[\phi]$ and $\tilde{\xi}[\tilde{\phi}]$. The functional form of f , in terms of the disentangling variables ξ and $\tilde{\xi}$, depends on the chosen observable and the initial state. The equation of motion of f is obtained from the Ito chain rule as given by Eq. (16) in the main text. This can be written as $\dot{f} = \Upsilon f$, where we define the linear operator

$$\Upsilon \equiv \sum_{ia} (A_i^a + \sum_{jb} B_{ij}^{ab} \phi_j^b) \frac{\partial}{\partial \xi_i^a} + \frac{1}{2} \sum_{ijab} \sum_{ck} B_{ik}^{ac} B_{jk}^{bc} \frac{\partial^2}{\partial \xi_i^a \partial \xi_j^b}. \quad (\text{E3})$$

For notational economy, the indices a and b run over $\{+, -, z\}$ and over both the $\xi, \tilde{\xi}$ variables. The analytical expression for the average $\langle d\mathcal{O}(t)/dt \rangle = \langle \dot{f} \rangle_{\phi, \tilde{\phi}}$ can be obtained by applying (E3) to the definition (E2) and averaging over the HS fields $\phi, \tilde{\phi}$:

$$\begin{aligned} \langle \dot{f} \rangle_{\phi, \tilde{\phi}} &= \left\langle \langle \psi_0 | \left(\Upsilon [\hat{U}^s(\tilde{\xi})]^\dagger \right) \hat{O} \hat{U}^s(\xi) | \psi_0 \rangle \right\rangle_{\phi, \tilde{\phi}} \\ &\quad + \left\langle \langle \psi_0 | [\hat{U}^s(\tilde{\xi})]^\dagger \hat{O} \left(\Upsilon \hat{U}^s(\xi) \right) | \psi_0 \rangle \right\rangle_{\phi, \tilde{\phi}}. \end{aligned} \quad (\text{E4})$$

Since $\langle \hat{U}^s \rangle_\phi = \hat{U}$, we can simplify (E4) using

$$\left\langle \Upsilon \hat{U}^s(\xi) \right\rangle_\phi = \left\langle \frac{d}{dt} \hat{U}^s(\xi) \right\rangle_\phi = -i\hat{H}\hat{U}. \quad (\text{E5})$$

This can also be verified by directly evaluating $\Upsilon \hat{U}^s(t)$ and using the commutation relations of $su(2)$. Similarly,

$$\left\langle \Upsilon [\hat{U}^s(\tilde{\xi})]^\dagger \right\rangle_{\tilde{\phi}} = \left\langle \frac{d}{dt} [\hat{U}^s(\tilde{\xi})]^\dagger \right\rangle_{\tilde{\phi}} = i\hat{U}^\dagger \hat{H}. \quad (\text{E6})$$

Using these identities, the equation of motion (E4) for $\langle \hat{O}(t) \rangle$ can be written as

$$\langle \psi_0 | \frac{d\hat{O}}{dt} | \psi_0 \rangle = \langle f \rangle_{\phi, \tilde{\phi}} = i \langle \psi_0 | \left(\hat{H} \hat{U}^\dagger \hat{O} \hat{U} - \hat{U}^\dagger \hat{O} \hat{U} \hat{H} \right) | \psi_0 \rangle. \quad (\text{E7})$$

This can be recognized as a matrix element of the Heisenberg equation of motion

$$\frac{d}{dt} \hat{O}(t) = i[\hat{H}, \hat{O}(t)]. \quad (\text{E8})$$

Such matrix elements give rise to a set of coupled first order ODEs, whose number in general grows exponentially

with the system size. Solving these ODEs is therefore equivalent to diagonalizing the Hamiltonian.

Appendix F: Building Blocks for Local Observables

As discussed in Section III, expectation values of products of local operators, starting from a product state, can be expressed in terms of stochastic averages over products of on-site ‘‘building blocks’’. This follows from the fact that the time-evolution operator can be factorized over lattice sites as $U(t) = \langle U^s(t) \rangle_\phi$ where $\hat{U}^s(t) \equiv \otimes_i \hat{U}_i^s(t)$. For example, if there are no spin operators in the observable \hat{O} at site i we may use the building blocks

$$\begin{aligned} \mathcal{B}_i^{\uparrow\uparrow} &\equiv {}_i \langle \uparrow | \hat{U}_i^s(\tilde{\xi})^\dagger \hat{U}_i^s(\xi) | \uparrow \rangle_i \\ &= e^{-\frac{\xi_i^z + \tilde{\xi}_i^{z*}}{2}} \left(e^{\xi_i^z + \tilde{\xi}_i^{z*}} + e^{\tilde{\xi}_i^{z*}} \xi_i^- \xi_i^+ + e^{\xi_i^z} \tilde{\xi}_i^{-*} \tilde{\xi}_i^+ + \xi_i^- \tilde{\xi}_i^{-*} (1 + \xi_i^+ \tilde{\xi}_i^{+*}) \right), \end{aligned} \quad (\text{F1a})$$

$$\mathcal{B}_i^{\uparrow\downarrow} \equiv {}_i \langle \uparrow | \hat{U}_i^s(\tilde{\xi})^\dagger \hat{U}_i^s(\xi) | \downarrow \rangle_i = e^{-\frac{\xi_i^z + \tilde{\xi}_i^{z*}}{2}} \left(\tilde{\xi}_i^{-*} + e^{\tilde{\xi}_i^{z*}} \xi_i^+ + \tilde{\xi}_i^{-*} \xi_i^+ \tilde{\xi}_i^{+*} \right), \quad (\text{F1b})$$

$$\mathcal{B}_i^{\downarrow\uparrow} \equiv {}_i \langle \downarrow | \hat{U}_i^s(\tilde{\xi})^\dagger \hat{U}_i^s(\xi) | \uparrow \rangle_i = e^{-\frac{\xi_i^z + \tilde{\xi}_i^{z*}}{2}} \left(\xi_i^- + e^{\xi_i^z} \tilde{\xi}_i^{+*} + \xi_i^- \xi_i^+ \tilde{\xi}_i^{+*} \right), \quad (\text{F1c})$$

$$\mathcal{B}_i^{\downarrow\downarrow} \equiv {}_i \langle \downarrow | \hat{U}_i^s(\tilde{\xi})^\dagger \hat{U}_i^s(\xi) | \downarrow \rangle_i = e^{-\frac{\xi_i^z + \tilde{\xi}_i^{z*}}{2}} (1 + \xi_i^+ \tilde{\xi}_i^{+*}), \quad (\text{F1d})$$

depending on the initial and final states. If the spin op-

erator S_i^z is present in \hat{O} we may use one of the following:

$$\mathcal{B}_i^{z\uparrow\uparrow} \equiv {}_i \langle \uparrow | \hat{U}_i^s(\tilde{\xi})^\dagger \hat{S}_i^z \hat{U}_i^s(\xi) | \uparrow \rangle_i = \frac{1}{2} e^{-\frac{\xi_i^z + \tilde{\xi}_i^{z*}}{2}} \left(e^{\xi_i^z + \tilde{\xi}_i^{z*}} + e^{\tilde{\xi}_i^{z*}} \xi_i^- \xi_i^+ + e^{\xi_i^z} \tilde{\xi}_i^{-*} \tilde{\xi}_i^+ + \xi_i^- \tilde{\xi}_i^{-*} (-1 + \xi_i^+ \tilde{\xi}_i^{+*}) \right), \quad (\text{F2a})$$

$$\mathcal{B}_i^{z\uparrow\downarrow} \equiv {}_i \langle \uparrow | \hat{U}_i^s(\tilde{\xi})^\dagger \hat{S}_i^z \hat{U}_i^s(\xi) | \downarrow \rangle_i = \frac{1}{2} e^{-\frac{\xi_i^z + \tilde{\xi}_i^{z*}}{2}} \left(-\tilde{\xi}_i^{-*} + e^{\tilde{\xi}_i^{z*}} \xi_i^+ + \tilde{\xi}_i^{-*} \xi_i^+ \tilde{\xi}_i^{+*} \right), \quad (\text{F2b})$$

$$\mathcal{B}_i^{z\downarrow\uparrow} \equiv {}_i \langle \downarrow | \hat{U}_i^s(\tilde{\xi})^\dagger \hat{S}_i^z \hat{U}_i^s(\xi) | \uparrow \rangle_i = \frac{1}{2} e^{-\frac{\xi_i^z + \tilde{\xi}_i^{z*}}{2}} \left(-\xi_i^- + e^{\xi_i^z} \tilde{\xi}_i^{+*} + \xi_i^- \xi_i^+ \tilde{\xi}_i^{+*} \right), \quad (\text{F2c})$$

$$\mathcal{B}_i^{z\downarrow\downarrow} \equiv {}_i \langle \downarrow | \hat{U}_i^s(\tilde{\xi})^\dagger \hat{S}_i^z \hat{U}_i^s(\xi) | \downarrow \rangle_i = \frac{1}{2} e^{-\frac{\xi_i^z + \tilde{\xi}_i^{z*}}{2}} (-1 + \xi_i^+ \tilde{\xi}_i^{+*}). \quad (\text{F2d})$$

Similarly, if the observable \hat{O} contains \hat{S}_i^+ , \hat{S}_i^- we may

use:

$$\mathcal{B}_i^{+\uparrow\uparrow} \equiv {}_i \langle \uparrow | \hat{U}_i^s(\tilde{\xi})^\dagger \hat{S}_i^+ \hat{U}_i^s(\xi) | \uparrow \rangle_i = e^{-\frac{\xi_i^z + \tilde{\xi}_i^{z*}}{2}} \xi_i^- \left((\tilde{\xi}_i^- \tilde{\xi}_i^+)^* + e^{\tilde{\xi}_i^{z*}} \right) \quad (\text{F3a})$$

$$\mathcal{B}_i^{+\uparrow\downarrow} \equiv {}_i \langle \uparrow | \hat{U}_i^s(\tilde{\xi})^\dagger \hat{S}_i^+ \hat{U}_i^s(\xi) | \downarrow \rangle_i = e^{-\frac{\xi_i^z + \tilde{\xi}_i^{z*}}{2}} \left((\tilde{\xi}_i^- \tilde{\xi}_i^+)^* + e^{\tilde{\xi}_i^{z*}} \right), \quad (\text{F3b})$$

$$\mathcal{B}_i^{+\downarrow\uparrow} \equiv {}_i \langle \downarrow | \hat{U}_i^s(\tilde{\xi})^\dagger \hat{S}_i^+ \hat{U}_i^s(\xi) | \uparrow \rangle_i = e^{-\frac{\xi_i^z + \tilde{\xi}_i^{z*}}{2}} \xi_i^- \tilde{\xi}_i^{+*}, \quad (\text{F3c})$$

$$\mathcal{B}_i^{+\downarrow\downarrow} \equiv {}_i \langle \downarrow | \hat{U}_i^s(\tilde{\xi})^\dagger \hat{S}_i^+ \hat{U}_i^s(\xi) | \downarrow \rangle_i = e^{-\frac{\xi_i^z + \tilde{\xi}_i^{z*}}{2}} \tilde{\xi}_i^{+*}. \quad (\text{F3d})$$

$$\mathcal{B}_i^{-\uparrow\uparrow} \equiv {}_i\langle \uparrow | \hat{U}_i^s(\tilde{\xi})^\dagger \hat{S}_i^- \hat{U}_i^s(\xi) | \uparrow \rangle_i = e^{-\frac{\tilde{\xi}_i^z + \xi_i^{z*}}{2}} \tilde{\xi}_i^{-*} \left(\xi_i^- \xi_i^+ + e^{\xi_i^z} \right), \quad (\text{F4a})$$

$$\mathcal{B}_i^{-\uparrow\downarrow} \equiv {}_i\langle \uparrow | \hat{U}_i^s(\tilde{\xi})^\dagger \hat{S}_i^- \hat{U}_i^s(\xi) | \downarrow \rangle_i = e^{-\frac{\tilde{\xi}_i^z + \xi_i^{z*}}{2}} \xi_i^+ \tilde{\xi}_i^{-*}, \quad (\text{F4b})$$

$$\mathcal{B}_i^{-\downarrow\uparrow} \equiv {}_i\langle \downarrow | \hat{U}_i^s(\tilde{\xi})^\dagger \hat{S}_i^- \hat{U}_i^s(\xi) | \uparrow \rangle_i = e^{-\frac{\tilde{\xi}_i^z + \xi_i^{z*}}{2}} \left(\xi_i^- \xi_i^+ + e^{\xi_i^z} \right), \quad (\text{F4c})$$

$$\mathcal{B}_i^{-\downarrow\downarrow} \equiv {}_i\langle \downarrow | \hat{U}_i^s(\tilde{\xi})^\dagger \hat{S}_i^- \hat{U}_i^s(\xi) | \downarrow \rangle_i = e^{-\frac{\tilde{\xi}_i^z + \xi_i^{z*}}{2}} \xi_i^+. \quad (\text{F4d})$$

For example, starting in the fully-polarized initial state $|\downarrow\rangle$ one readily obtains

$$\langle \hat{S}_i^x(t) \rangle = \frac{1}{2} \langle \hat{S}_i^+ + \hat{S}_i^- \rangle = \frac{1}{2} \langle (\mathcal{B}_i^{+\downarrow\downarrow} + \mathcal{B}_i^{-\downarrow\downarrow}) \prod_{j \neq i} \mathcal{B}_j^{\downarrow\downarrow} \rangle_{\phi, \tilde{\phi}}. \quad (\text{F5})$$

Using the above results one arrives at the exact formula

$$\langle \hat{S}_i^x(t) \rangle = \frac{1}{2} \left\langle e^{-\sum_j \left(\frac{\xi_j^z + \tilde{\xi}_j^{z*}}{2} \right)} (\xi_i^+ + \tilde{\xi}_i^{+*}) \prod_{j \neq i} (1 + \xi_j^+ \tilde{\xi}_j^{+*}) \right\rangle_{\phi, \tilde{\phi}}. \quad (\text{F6})$$

Similarly,

$$\langle \hat{S}_i^y(t) \rangle = \frac{i}{2} \left\langle e^{-\sum_j \left(\frac{\xi_j^z + \tilde{\xi}_j^{z*}}{2} \right)} (\xi_i^+ - \tilde{\xi}_i^{+*}) \prod_{j \neq i} (1 + \xi_j^+ \tilde{\xi}_j^{+*}) \right\rangle_{\phi, \tilde{\phi}}. \quad (\text{F7})$$

The result for $\langle \hat{S}_i^z(t) \rangle$ is given by (21) in the main text.

Appendix G: Ising Stochastic Differential Equations

As we discussed in Section IV, the Ito SDEs for the quantum Ising model are given by Eq. (26), which we repeat here for convenience:

$$-i\dot{\xi}_j^+ = \frac{\Gamma}{2} (1 - \xi_j^{+2}) + \xi_j^+ \sum_k O_{jk} \phi_k / \sqrt{i}, \quad (\text{G1a})$$

$$-i\dot{\xi}_j^z = -\Gamma \xi_j^+ + \sum_k O_{jk} \phi_k / \sqrt{i}, \quad (\text{G1b})$$

$$-i\dot{\xi}_j^- = \frac{\Gamma}{2} \exp \xi_j^z. \quad (\text{G1c})$$

It is readily seen that the disentangling variable ξ_j^+ plays a particularly important role for the quantum dynamics in this parameterization: as we will discuss, ξ_j^+ vanishes identically in the classical limit $\Gamma = 0$, and it is the only disentangling variable that is not dependent on the others, as follows from (G1a). Once ξ_j^+ is known, ξ_j^z can be obtained by integrating (G1b) with respect to time. In turn, ξ_j^- has a deterministic dependence on ξ_j^z , as follows from (G1c). The non-linearity of the equation of motion (G1a) for ξ_j^+ , renders it non-trivial to solve. However, exact solutions to the full set of SDEs (G1) are readily

obtained in the classical limit with $\Gamma = 0$, and in the non-interacting limit with $J = 0$. We consider each below.

In the classical limit with $\Gamma = 0$, the equation of motion for $\xi_j^+(t)$ becomes linear. Due to the initial condition $\xi_j^+(0) = 0$ one obtains the trivial solution $\xi_j^+(t) = 0$. Similarly, $\xi_j^-(t) = 0$. The variable $\xi_j^z(t)$ undergoes Brownian motion and its time-evolution can be computed as

$$\xi_j^z(t) = i \sum_k O_{jk} \int_0^t dt' \phi_k(t') = \sqrt{i} \sum_k O_{jk} W_k(t). \quad (\text{G2})$$

The quantities $W_k(t)$ are a set of N independent standard Wiener processes, which can be numerically generated as

$$W_k(t) = \sqrt{t} \mathcal{N}(0, 1), \quad (\text{G3})$$

where $\mathcal{N}(0, 1)$ is a random number extracted from a zero-mean, unit-variance Gaussian distribution. In the classical limit with $\Gamma = 0$, there is no dynamics; this result can be recovered by substituting (G2) into the stochastic expressions for observables. For example, for the Loschmidt amplitude (19) and the magnetization (obtained using the building blocks in Appendix F) one obtains

$$|A(t)| = 1, \quad (\text{G4})$$

$$\langle \hat{S}_j^z(t) \rangle = \langle \hat{S}_j^z(0) \rangle, \quad (\text{G5})$$

for any initial condition. For example, for quantum quenches from the fully-polarized initial state $|\downarrow\rangle$, the Loschmidt amplitude and magnetization can be obtained by substituting (G2) and $\xi_i^+ = 0$ into (28) and (21):

$$A(t) = \left\langle \exp \left(\frac{(i+1)}{2} \sqrt{NJ} W_1(t) \right) \right\rangle_{\phi}, \quad (\text{G6})$$

$$\mathcal{M}(t) = -\frac{1}{2} \left\langle \exp \left(\frac{\sqrt{NJ}}{2} [(1+i)W_1(t) + (1-i)\tilde{W}_1(t)] \right) \right\rangle_{\phi, \tilde{\phi}}, \quad (\text{G7})$$

where $W_1(t)$ and $\tilde{W}_1(t)$ are independent Wiener processes obtained as in Eq. (G3). Averaging the above equations with respect to the noises ϕ , one obtains the results (G4) and (G5). From (G2), one can also calculate the variance of the stochastic functions f_A and $f_{\mathcal{M}}$ corresponding to these observables, via $A(t) \equiv \langle f_A \rangle_{\phi}$ and

$\mathcal{M}(t) \equiv \langle f_{\mathcal{M}} \rangle_{\phi, \bar{\phi}}$. One obtains

$$\sigma^2(f_A) = e^{\frac{NtJ}{2}} - 1, \quad (\text{G8})$$

$$\sigma^2(f_{\mathcal{M}}) = \frac{1}{4} (e^{NtJ} - 1). \quad (\text{G9})$$

In both cases, the variance grows exponentially with time and the system size. The similar functional form of the Loschmidt amplitude (19) and the magnetization (21), which both involve exponential factors of $e^{-\sum_i \xi_i^z(t)/2}$, leads to similar behavior for the fluctuations. An extra factor of two is present in the exponent for the magnetization due to the presence of two Hubbard–Stratonovich transformations for local observables. The presence of the exponential factors is suggestive of the exponential growth of fluctuations even for non-zero Γ . This is observed numerically and is discussed in the main text.

In the non-interacting limit with $J = 0$ the equations of motion for the disentangling variables become deterministic, as $O_{jk} = 0$. These can be solved analytically:

$$\xi_j^+(t) = i \tan(\Gamma t/2), \quad (\text{G10a})$$

$$\xi_j^z(t) = -2 \log \cos(\Gamma t/2), \quad (\text{G10b})$$

$$\xi_j^-(t) = i \tan(\Gamma t/2). \quad (\text{G10c})$$

As expected, (G10) parameterizes the precession of a single spin in a magnetic field applied along the x -direction. This can be seen by writing the time-evolved state $|\psi(t)\rangle = \hat{U}(t)|_{J=0}|\psi(0)\rangle$ for product-state initial conditions $|\psi(0)\rangle = \otimes_j (a_j |\uparrow\rangle_j + b_j |\downarrow\rangle_j)$ with $|a_j|^2 + |b_j|^2 = 1$, using the values of ξ given in (G10). This yields

$$|\psi(t)\rangle = \bigotimes_j \begin{pmatrix} a_j \cos(\Gamma t/2) - ib_j \sin(\Gamma t/2) \\ -ia_j \sin(\Gamma t/2) + b_j \cos(\Gamma t/2) \end{pmatrix}. \quad (\text{G11})$$

Appendix H: Moments of the Disentangling Variables

As we noted in Section V C, certain averages of the classical disentangling variables are identically zero for all times. Here, we go further and demonstrate that a set of monomials in $R_i \equiv \text{Re}(\xi_i^+)$ and $I_i \equiv \text{Im}(\xi_i^+)$ have vanishing averages for all t . To see this we note that the coupled SDEs for R_i and I_i can be obtained by combining Eq. (G1a) with its complex conjugate:

$$\dot{R}_i(t) = \Gamma R_i I_i + \frac{\sqrt{2}}{2} [R_i(O_{Ri} - O_{Ii}) - I_i(O_{Ri} + O_{Ii})] \phi \quad (\text{H1a})$$

$$\dot{I}_i(t) = \frac{\Gamma}{2} (1 - R_i^2 + I_i^2) + \frac{\sqrt{2}}{2} [R_i(O_{Ri} + O_{Ii}) + I_i(O_{Ri} - O_{Ii})] \phi \quad (\text{H1b})$$

In the above, we have introduced the shorthand notation $O_{Ri}\phi \equiv \sum_j (O_R)_{ij} \phi_j$, where $(O_R)_{ij} \equiv \text{Re}(O_{ij})$, and similarly for O_I . The identities we wish to show are most easily proved by introducing a convenient formal notation; this makes it simpler to analyze the system of ODEs which arise from averaging the SDEs. In particular, let us represent the classical average of a given monomial $\langle R_i^n I_i^m \rangle_{\phi}$ as a *state* $|n_i, m_i\rangle$. To compute the time-evolution of this state, one applies the Ito chain rule (16); this requires differentiating with respect to R_i and I_i . Due to (H1), each differentiation with respect to R_i (I_i) decreases n_i (m_i) by 1, and annihilates a state where n_i (m_i) is equal to zero. This suggests that we can formally represent derivatives as *annihilation operators* $\hat{a}_{Ri} \equiv \frac{\partial}{\partial R_i}$, $\hat{a}_{Ii} \equiv \frac{\partial}{\partial I_i}$ satisfying

$$\hat{a}_{Ri}|n, m\rangle = n_i |n_i - 1, m_i\rangle, \quad (\text{H2a})$$

$$\hat{a}_{Ii}|n, m\rangle = m_i |n_i, m_i - 1\rangle. \quad (\text{H2b})$$

Following the same line of reasoning, we can represent R_i and I_i themselves as *creation operators* satisfying

$$\hat{a}_{Ri}^{\dagger}|n_i, m_i\rangle = |n_i + 1, m_i\rangle, \quad (\text{H3a})$$

$$\hat{a}_{Ii}^{\dagger}|n_i, m_i\rangle = |n_i, m_i + 1\rangle. \quad (\text{H3b})$$

It can be seen that the operators satisfy bosonic commutation relations $[\hat{a}_X, \hat{a}_{X'}^{\dagger}] = \delta_{XX'}$ where $X, X' \in \{R_i, I_i\}$. We can use the notations introduced above to compactly write the equation of motion for a general state $|n_i, m_i\rangle = \langle R_i^n I_i^m \rangle_{\phi}$, obtained via the Ito chain rule, as

$$\frac{d}{dt}|n_i, m_i\rangle = -\hat{H}_i|n_i, m_i\rangle \quad (\text{H4})$$

where we have defined an effective Hamiltonian \hat{H}_i :

$$\begin{aligned} \hat{H}_i \equiv & \Gamma \hat{a}_{Ri}^{\dagger} \hat{a}_{Ii}^{\dagger} \hat{a}_{Ri} + \frac{\Gamma}{2} \left(1 - \hat{a}_{Ri}^{\dagger} \hat{a}_{Ri} + \hat{a}_{Ii}^{\dagger} \hat{a}_{Ii} \right) \hat{a}_{Ii} \\ & + \frac{1}{2} (O_I O_I^T + O_R O_R^T)_{ii} (\hat{a}_{Ri}^{\dagger} \hat{a}_{Ri} + \hat{a}_{Ii}^{\dagger} \hat{a}_{Ii}) (\hat{a}_{Ri} \hat{a}_{Ri} + \hat{a}_{Ii} \hat{a}_{Ii}). \end{aligned} \quad (\text{H5})$$

In deriving Eq. (H5), we used the Ito calculus property $\langle f(t)\phi(t) \rangle_{\phi} = 0$, and the properties of O_R and O_I given in Appendix B. In Eq. (H4), the time-evolution of a general classical average $\langle R_i^n(t) I_i^m(t) \rangle_{\phi}$ has been cast in a form that is reminiscent of a Euclidean Schrödinger equation, where the real-time variable t plays the role of an imaginary-time variable. The notations introduced above allow us to obtain an infinite number of identities for monomials in R_i, I_i . As it can be seen from (H5), the Hamiltonian does not contain any term that raises or lowers the index n_i of a state $|n_i, m_i\rangle$ by an odd number. Hence, states with odd and even n_i belong to separate even and odd subspaces \mathcal{H}_e and \mathcal{H}_o . At $t = 0$, the initial condition $\xi_i^+(0) = 0$ translates into the initial conditions $|n_i, m_i\rangle = \delta_{n_i, 0} \delta_{m_i, 0}$. Since $|0, 0\rangle \equiv |1\rangle_{\phi}$ does not belong to the odd subspace \mathcal{H}_o , all states $|n_i, m_i\rangle \in \mathcal{H}_o$ vanish identically at all times. This finding can be expressed as

$$\langle R_i^n(t) I_i^m(t) \rangle_{\phi} = 0, \quad \forall \quad n \text{ odd}. \quad (\text{H6})$$

This provides an analytical proof of the numerical observation that $\text{Re}\langle\xi_i^+(t)\rangle_\phi$ vanishes at all times, as we previously reported in Ref. [34]. Thus far, we have focused on moments involving variables at a single site i . The multi-site generalization is straightforward and is analogous to the construction of a many-site Fock space from a collection of single-site ones. Creation and annihilation operators are defined analogously to the same-site case; from their definition, it is clear that operators acting at different sites commute, since they are just multiplications or differentiations by independent variables. Of particular interest is the case of monomials involving two sites $i \neq j$, associated with two times t_i, t_j . States can be defined as

$$\left\langle R_i^{n_i}(t_i)I_i^{m_i}(t_i)R_j^{n_j}(t_j)I_j^{m_j}(t_j) \right\rangle_\phi \equiv \left| (n_i, m_i, t_i)_i; (n_j, m_j, t_j)_j \right\rangle. \quad (\text{H7})$$

Consider, for example, the evolution of the state with respect to t_i . For $t_i \neq t_j$, this is given by Eq. (H4) where the state is replaced by (H7). For $t_j = t_i$, the effective

Hamiltonian becomes

$$\begin{aligned} \hat{H}_2 &= \hat{H}_i + \hat{H}_j \\ &+ \frac{1}{2}(O_I O_I^T + O_R O_R^T)_{ij}(\hat{a}_{Ri}^\dagger \hat{a}_{Rj}^\dagger + \hat{a}_{Ii}^\dagger \hat{a}_{Ij}^\dagger)(\hat{a}_{Ri} \hat{a}_{Rj} + \hat{a}_{Ii} \hat{a}_{Ij}) \\ &+ \frac{1}{2}(O_I O_I^T + O_R O_R^T)_{ij}(\hat{a}_{Ri}^\dagger \hat{a}_{Ij}^\dagger - \hat{a}_{Ii}^\dagger \hat{a}_{Rj}^\dagger)(\hat{a}_{Ri} \hat{a}_{Ij} - \hat{a}_{Ii} \hat{a}_{Rj}) \\ &+ \mathcal{J}_{ij}(\hat{a}_{Ri}^\dagger \hat{a}_{Rj}^\dagger - \hat{a}_{Ii}^\dagger \hat{a}_{Ij}^\dagger)(\hat{a}_{Ri} \hat{a}_{Ij} + \hat{a}_{Ii} \hat{a}_{Rj}) \\ &- \mathcal{J}_{ij}(\hat{a}_{Ri}^\dagger \hat{a}_{Ij}^\dagger + \hat{a}_{Ii}^\dagger \hat{a}_{Rj}^\dagger)(\hat{a}_{Ri} \hat{a}_{Rj} - \hat{a}_{Ii} \hat{a}_{Ij}). \end{aligned} \quad (\text{H8})$$

Eq. (H8) allows us to generalize the result (H6) for monomials involving two sites. Consider the total number of R factors in a given monomial, $n = n_i + n_j$. When i and j are not nearest neighbors, the last two terms in (H8) vanish, and both the Hamiltonians (H5) and (H8) conserve the overall evenness or oddness of n . By the same argument as in the one-site case, states with odd n must therefore vanish for all t_i, t_j . This finding can be used to prove the vanishing of $\text{Im} C_n^{zz}(t)$ with $n \geq 2$, as defined in Eq. (40) and numerically studied in Section V. Using Ito calculus, we find that $C_n^{zz}(t)$ is given by

$$C_n^{zz}(t) = -\Gamma \sum_i \int_0^t \int_0^t dt_1 dt_2 [\langle \xi_i^+(t_1) \xi_{i+n}^+(t_2) \rangle_\phi - \langle \xi_i^+(t_1) \rangle_\phi \langle \xi_{i+n}^+(t_2) \rangle_\phi]. \quad (\text{H9})$$

By Eq. (H6), we know that $\langle \xi_i^+(t) \rangle$ is purely imaginary for all i, t , such that the second contribution to Eq. (H9) is real-valued. The first contribution involves

$$\begin{aligned} \langle \xi_i^+(t_1) \xi_{i+n}^+(t_2) \rangle_\phi &= \langle R_i(t_1) R_{i+n}(t_2) \rangle_\phi - \langle I_i(t_1) I_{i+n}(t_2) \rangle_\phi \\ &+ i \langle R_i(t_1) I_{i+n}(t_2) \rangle_\phi + i \langle I_i(t_1) R_{i+n}(t_2) \rangle_\phi. \end{aligned} \quad (\text{H10})$$

It can be seen that the imaginary part of $\langle \xi_i^+(t_1) \xi_{i+n}^+(t_2) \rangle_\phi$ features only monomials with odd n , which vanish for any t_1, t_2 by the previous argument. Thus, the connected correlation function $C_n^{zz}(t)$ with

$n \geq 2$ must be real valued. The operator description of the evolution of moments introduced in this Section allows us to identify vanishing expectation values in a transparent way, without solving the SDEs (G1). The presence of identically vanishing moments suggests that the Ising SDEs may contain a degree of redundancy, and that it may be possible to reduce them to a simpler form which automatically takes into account these vanishing averages. The operator formalism employed to find the vanishing moments provides a rather general alternative viewpoint, which may turn out to be a useful tool for future developments.